Title
A Novel Analysis of Skeletal Asymmetry Utilizing 3D CBCT Technology: The Ulrich Analysis

Author
Ulrich, Beau

Publication Date
2012

Peer reviewed|Thesis/dissertation

A Novel Analysis of Skeletal Asymmetry Utilizing 3D CBCT Technology: The Ulrich Analysis

by

Beau Ulrich, DDS

THESIS

Submitted in partial satisfaction of the requirements for the degree of

MASTER OF SCIENCE

in

Oral and Craniofacial Sciences

in the

GRADUATE DIVISION

of the

UNIVERSITY OF CALIFORNIA, SAN FRANCISCO

DEDICATION

I would like to dedicate this thesis to my family. As my organized and institutionalized educational career draws to a close, you have been the foundational support that has allowed me to progress and achieve such great things while keeping myself emotionally and physically grounded. You have been my role models, my best friends, my cheering section and most of all, my inspiration to attain all that I have. I cannot thank you enough for the wisdom you instilled in me, nor the drive you taught me; I would not be where I am without you.

ACKNOWLEDGEMENTS

I would like to acknowledge a few key individuals who made this project and its development possible. Dr. James Chen has enabled an inexperienced author to properly describe and validate his findings through statistical analysis and been invaluable in the fabrication and contribution to this literary work. Dr. Ib Nielsen, with his unparalleled knowledge of orthodontics, has contributed an insurmountable amount of knowledge to balance an author's somewhat eager technological attitude and verbose nature with historical perspective and concise ideologies. Dr. John Huang, thank you for your support through the clinical and academic portion of the orthodontic program, as your attitude and familiarity with the technological forefronts of imaging and its integration with orthodontics continues to encourage greatness and inspire clinicians to further the field of orthodontics. And Dr. Art Miller, you have been the person responsible for such innovative and creative direction that allowed the construction of the Asymmetry Analysis and brought key features to the drawing table that would enhance the impact and importance of such a tool. Thank you all for helping to construct this thesis and project, whatever direction or influence it may have on future generations of orthodontists.

ABSTRACT

Introduction: Proper diagnosis and treatment planning is essential to the outcome of orthodontic therapy with accurate diagnostic records being the pinnacle of that process. Previously, two-dimensional imagery has been the standard in analyzing or visualizing a patient for skeletal asymmetries but has numerous limiting factors. The limitations that two dimensional analyses face can be solved by the use of three-dimensional cone beam computed tomography (CBCT) when combined with an efficient and relevant analysis. The purpose of this study was to design a novel analysis of asymmetry utilizing CBCT that could be used in a standard orthodontic diagnostic analysis.

Methods: CBCT images of 35 patients from the UCSF Orthodontic Clinic were used for development of the analysis. A pilot study with 5 patients having marked asymmetries was traced at 3 different time points to aid in landmark verification and assess reliability. A series of landmarks sharing commonalities with those used in two-dimensional cephalometric analysis were applied. A Pearson Correlation Coefficient with Bonferonni correction as well as a Bland-Altman test for reproducibility was applied for the three timepoints on five different patients to test intraobserver reliability. 10 patients with a molar Class I malocclusion, 10 patients with CII malocclusions, and 10 with CIII malocclusions were used to create a sample of patients with the applied orientation method and asymmetry analysis.

Results: Landmark identification was found to be reproducible with only a weak statistical difference in landmark identification. No statistically significant differences were found between any landmarks and their different timepoint selections, particularly those points essential to the establishment of the analysis axis ($p<.05$). The index provided a quantitative assessment in three planes for both numerical and visual evidence of asymmetry.

Conclusions: The Ulrich Orthodontic Asymmetry analysis, combined with reliable and reproducible landmark selection, allows for successful quantitative assessment of asymmetry identification in both 2-dimensional and 3-dimensional visualizations and may provide a standard diagnostic tool to be used with patients seeking orthodontic treatment.

Keywords: three-dimensional imaging, cone-beam CT, CBCT, craniofacial skeleton, asymmetry, three-dimensional analysis

Table of Contents

INTRODUCTION

In all fields of dentistry, proper diagnosis and treatment planning is essential to a successful outcome of an applied therapy. Without accurate knowledge of existing problems or complications, therapeutic results could garner less than satisfactory results. In orthodontics, complete diagnostic records are the pinnacle of the treatment planning process, providing all significant physical information with which the patient presents.[1] Clinical observation and photographs are limited to superficial information, while radiographs continue to support the basis of hard tissue assessment and analysis.

Two-dimensional radiographic imaging has been the foundation for orthodontics for roughly half a century, with lateral cephalograms and panoramic radiographs constituting the basic standard of care in x-ray imaging for orthodontics[2]. Three-dimensional imagery is slowly becoming the standard within the clinical world of orthodontics. With more than 3,000 cone beam computed tomography (CBCT) machines now installed across the United States, 3-dimensional imaging is finding a place in the dental community[3]. Analysis of this CBCT data is currently under development, but investigators and clinicians continue to argue if the orthodontic clinician should use CBCT on a regular basis and under which conditions[4]. Associated cost[5] and radiation dosage are still arguable points when speaking of 3D CBCT imaging and the cost/benefit ratio in the field of dentistry[1, 6]. Despite such controversy, most current graduates from orthodontic programs around the nation receive some experience on reading and incorporating three-dimensional imagery into treatment planning and as a tool to aid in orthodontic diagnosis. The majority of orthodontic residencies provide

courses and direct education with CBCT to support the training of residents with the technology, albeit, in many different capacities[7]. In a recent survey by Smith *et al.,* it was shown that 83.3% of United States postgraduate orthodontic residencies have access to 3D imaging when it is necessary as an adjunct in diagnostics while 73.3% if the orthodontic programs indicated regular use[7].

Until ten years ago, most private orthodontists had little exposure to three-dimensional imaging, and even less were trained to manipulate and work with this type of visual data analysis.[8] With the reduction in cost of many CBCT machines, private practitioners are now beginning to incorporate these apparati into their offices. The mobilization of such technology combined with the wealth of knowledge that can be gleaned from its use, opens doors to new analysis that once were impossible with conventional two-dimensional imaging.

Many two-dimensional analyses exist to identify asymmetries. With multiple overlying structures and the absence of depth when attempting to locate landmarks, validity of these analyses is limited when trying to isolate areas of asymmetry or even evaluate their magnitude.[9] Due to overlapping structures and distortion that can develop due to patient placement, the accuracy of such analysis can come into question. [10]

All two-dimensional images suffer from multiple drawbacks including differential enlargement of structures, inability to assess depth, inaccuracy of direct measurement, and multiple overlying structures that can create difficulty in structural identification. 3D CBCT images alleviate most if not all of these issues while introducing their own complexities into

the mixture.[2, 11] Hard tissue structures and measurements have been found to be accurately represented by CBCT images with high reliability and accuracy.[12] It has even been corroborated in many studies that most landmarks traditionally identifiable in two-dimensional images can be identified in CBCT images with a high level of success.[8, 13]

Few studies have utilized CBCT to develop measurements to identify, quantify, and isolate the presence and severity of a skeletal asymmetry. The presence of such asymmetries can sometimes be difficult to localize due to multiple asymmetric areas and compensation.[14] The goal of this study is to develop an index of skeletal asymmetry utilizing CBCT to diagnose and quantify aberrations in bilateral symmetry. This index is developed for the orthodontic clinician with access to cone beam imagining, allowing the clinician to easily, and readily, identify and measure a patient's skeletal asymmetry. It is an index designed and based on skeletal landmarks, independent of rendering software orientation, thus allowing universal plane coordination and identification.

MATERIALS AND METHODS

Study Design

The study was a retrospective study, which consisted of and initial 5 test subjects with marked asymmetries, followed by 30 subjects selected at random from the patient population at the University of California San Francisco Orthodontic Clinic. This sample is the first stage to establishing a bank or library of subjects and consisted of 10 subjects with a Class I molar (CI) molar malocclusion, 10 with a CII malocclusion, and 10 with a CIII malocclusion.

The subjects were selected consecutively by the first 10 subjects fitting the malocclusion in which initial records were taken after July 2011. Molar classification was determined based on visual inspection and classification of the rendered volume in the computer software. Only patients that acquired complete records, including a full 12" CBCT scan, dental models, and impressions were included. Those with partial or incomplete records, phase I records, or those with appliances already in place were excluded from the study. All subjects had previously signed an informed consent acknowledging that their records could be used anonymously for university studies, including x-rays, CBCT images, photos and plaster models.

CBCT Imaging

Each patient had a full 12" CBCT scan as part of his or her beginning records on a Hitachi MercuRay (Hitachi, Tokyo) Cone Beam machine which was later rendered in InVivo Anatomage (San Jose, CA, version 5.1.6), software. All CBCT 3D tracings of patients were accomplished using InVivo Anatomage's subroutine, 3D Analysis software. A pilot study consisting of 5 subjects with marked asymmetries were used to establish validity of the index as well as assess intra-observer error in landmark identification and reproducibility. All subjects had landmarks initially identified in Anatomage software. Due to the time constraints of designing and programming the analysis and applying landmark verification over three timepoints, as well as constricting a banked population of 30 other patients, only 5 subjects were chosen to conclude the pilot study. All 5 pilot study subjects had the landmark identification repeated a second and third time with at least three weeks between sessions. Pilot study subjects were chosen randomly from a pool of subjects in which five orthodontic

resident volunteered one patient in which they felt had a clinically marked skeletal asymmetry.

Orientation

In order to negate the effect of the software orienting the head based on a proprietary algorithm, an axis needed to be established based on bony landmarks with sella set as the origin. With the advent of an individually established axes based on bony landmarks, any software could potentially repeat these axes (rather than the software orienting the skull) allowing for universal use of such analysis. To orient the patient's skull properly in the software with sella at the origin and a more intuitive positive and negative description of the x, y, and z axes, the mid-sagittal plane was defined first, followed by the horizontal plane and lastly, the vertical plane. All landmark points used to define the plane axis had to be traced prior to any other points in order to provide proper orientation of the patient.

In the InVivo software, before beginning any tracing tasks, the orientation had to be defined by selecting "Create Tracing", followed by clicking "Setup" that appears under the Tracing Tasks Menu. A Tracing Guide menu appeared so that the investigator could select a coordinate system based on picking landmarks that then could be defined by clicking the "Change" button directly to the right. The Define Coordinate System menu popped up at which point the investigator began to customize the orientation (Figure 1).

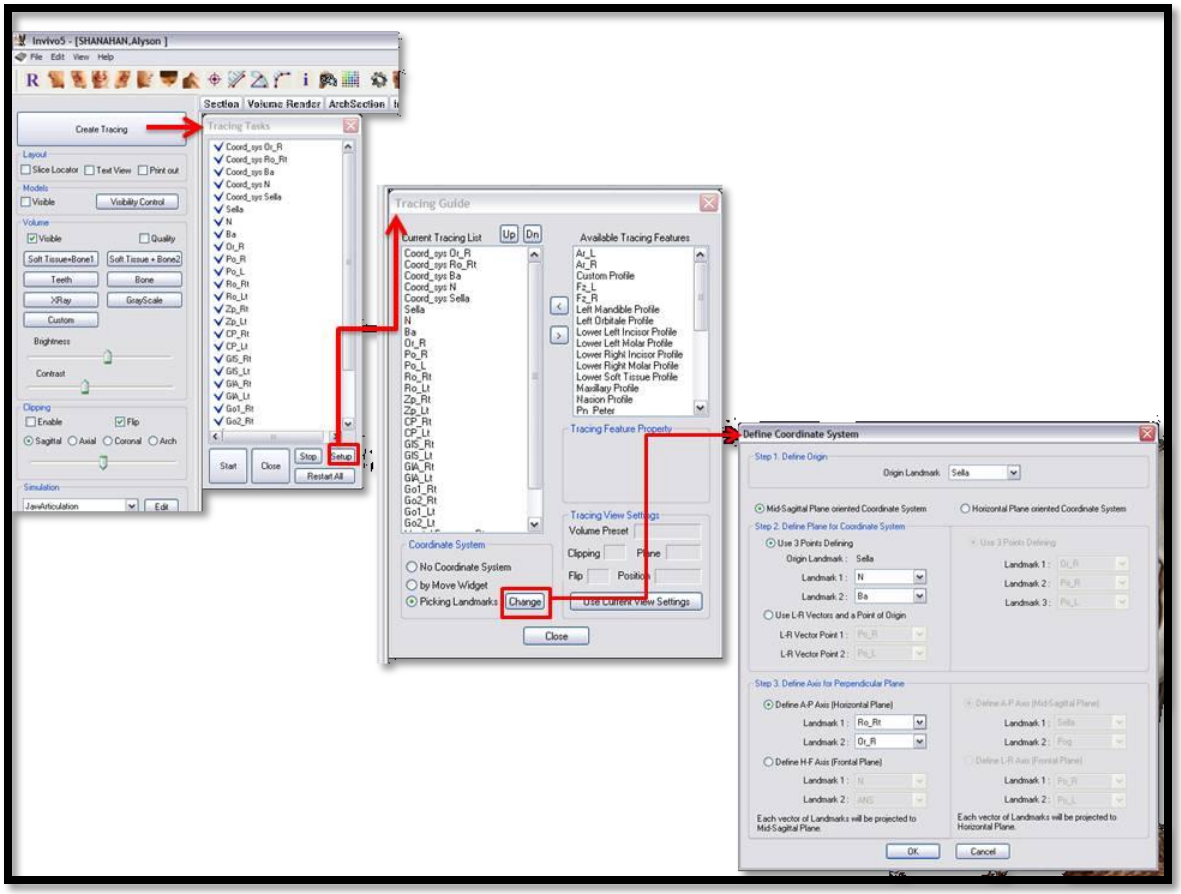

Figure 1: Example of the three window panels used for the initial steps to set up cephalometric x, y, and z axes and origin.

The mid-sagittal plane was defined based on three points that divided the head into a left/right orientation, creating a plane along the z-axis (Figure 2). After locating Sella for the origin point, Basion and Nasion were selected.

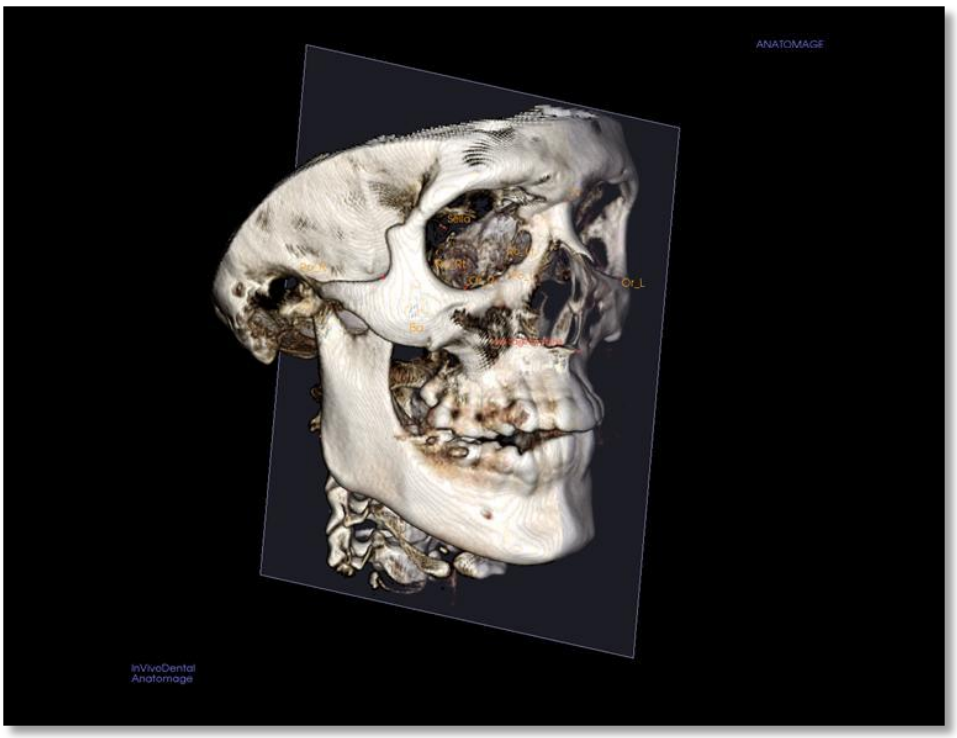

Figure 2: Example of the first plane that is constructed, the mid-sagittal plane, that is projected across three points of nasion, basion, and sella.

The horizontal plane was based on a vector projection of two points perpendicular to the mid-sagittal plane, creating a superior/inferior relation along the y-axial plane (Figure 3). Due to limitations in the software's ability to properly orientate the plane based on bilateral points, two ipsilateral points of foramen rotundum right and right orbitale were chosen.

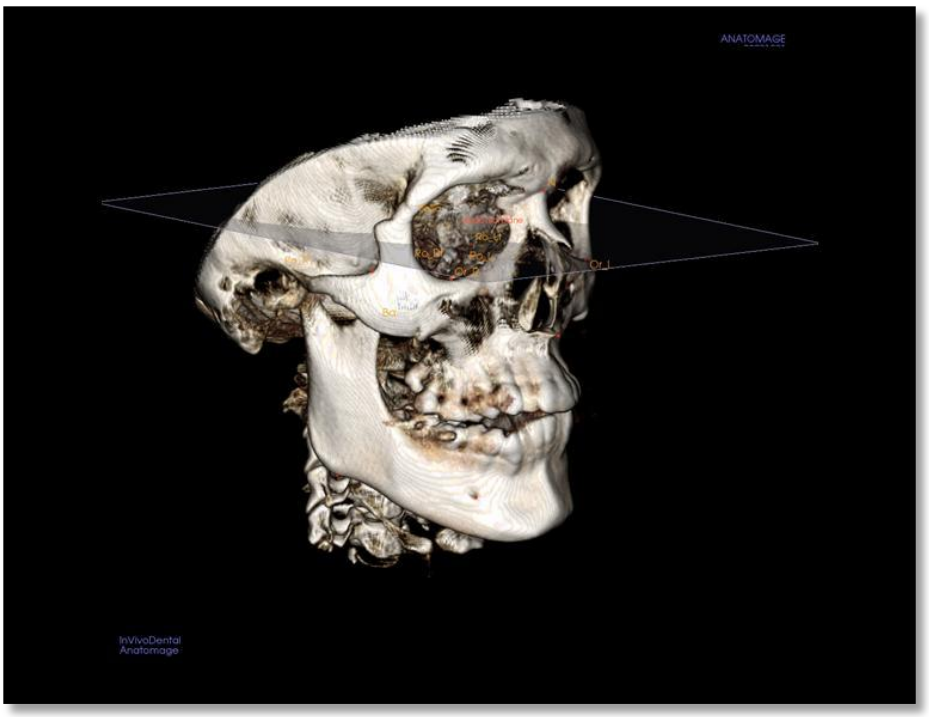

Figure 3: Projection of horizontal plane placed tangent to the mid-sagittal plane and passing through right orbitale.

A third plane, the frontal plane, was automatically created based on perpendicular projections from the mid-sagittal plane and the vertical planes (Figure 4). This allowed for an anterior/posterior relationship to be established utilizing a plane based on the x-axial coordinate plane originating at sella (Figure 5).

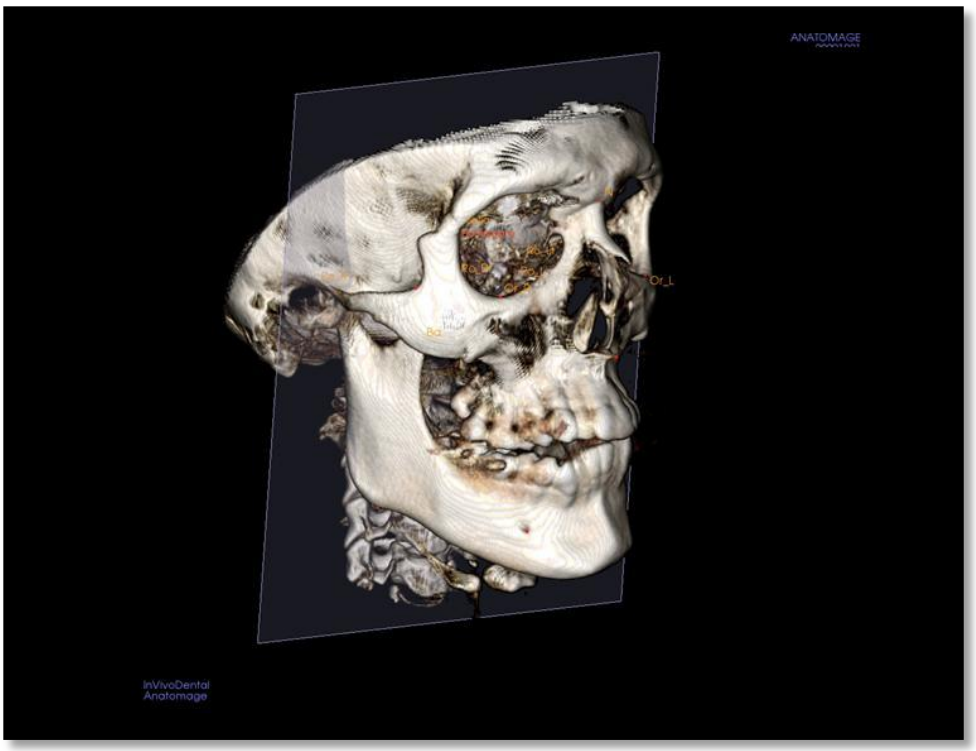

Figure 4: Example of the frontal plane that is projected tangent to both the mid-sagittal plane and the frontal plane, with the origin placed at sella.

Once the coordinate system was defined, the Tracing Tasks were initiated by selecting "Start". The patient data was then automatically orientated based on the planer construction defined by the user and independent of the software's reconstruction algorithm.

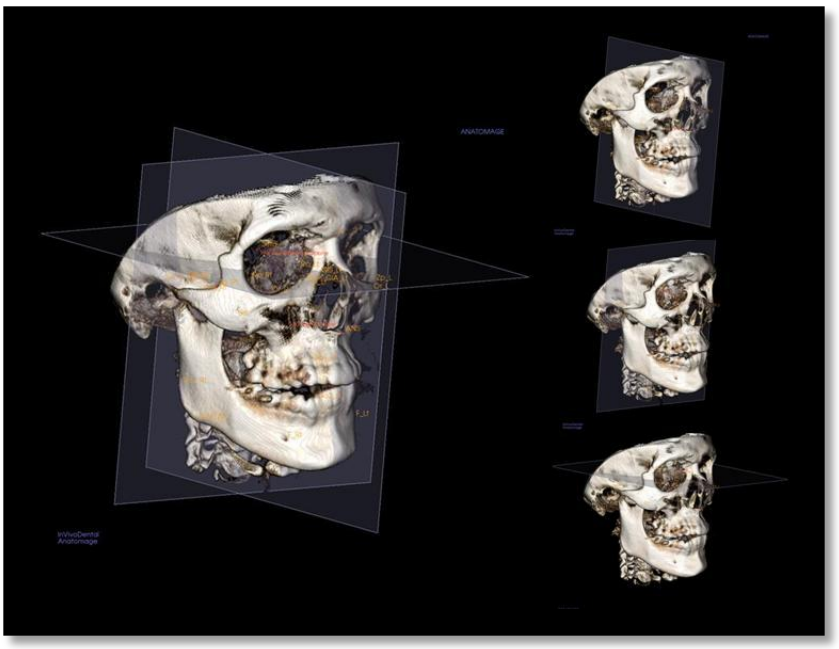

Figure 5: Three-dimensional volumetric view of one subject in which the three different planes, sagittal, horizontal, and frontal, are depicted with the origin at sella.

Landmarks and Landmark Selection

Before any of the patients could be traced using the index, parameters of the index had to be established and logged into the software tracing tasks using the subroutine, 3-D Analysis. In the 3-D Analysis tracing module, custom landmarks were established via the landmark tab under the settings icon. Each landmark was given a "Group" classification based on its location in a region such as the point ANS being placed under the group classification of "Maxillary" (Table 1). Once the patient's CBCT data was available, the 3D Analysis module was selected, and the Asymmetry Analysis that was developed as part of this study, was selected.

Landmarks were chosen for purposes of creating a repeatable set of axis as well as creating bilateral measurements that would allow the operator to identify and evaluate the extent of existing asymmetries of the patient. Landmarks that were judged to be more common

landmarks used in 2-dimensional cephalometry were chosen for their already familiar usage to the clinician.

Three reliable points had to be chosen, based on the computer software's defining parameters, to initiate the construction of an axis (establishment of the x-axis). A point on the mid-cranial base was identified as the origin, one which was unchanging to allow for the possibility of future superimpositions. Considering the completion of natural growth in the mid-cranial base at roughly 8 years of age[15], and the minimal change in growth of its surrounding structures, sella or sella prime would be expected to be predictable in its position and cessation in growth as well as reliable in its identification.[16] A study by Lagravère *et al.,* revealed that sella was reproducibly identifiable especially along the x-axis, which is particularly important if any vector were projected through the point, such as the establishment of the vertical x-plane. A study by Schlicher *et al.,* found that out of 32 skeletal landmarks on three-dimensional tracings with multiple raters, Sella was the most reliable with a 0.50-mm mean deviation overall and only a 0.14-mm deviation along the x-axis.[17] The Lagravère *et al.*, study also verified nasion as reproducible with minimal error (less than 1-mm) in either the x or y planes.[16] Schlicher *et al.,* also identified basion as the second most reliable skeletal landmark with a minimal 0.32-mm deviation along the x-axis, lending it as a reproducible point for establishment of the basis of the orientation axis.[17]

Once landmarks that established the basis of the axis were selected, points that could be found bilaterally on the eye orbits, external auditory meatus, the midface, and lower face were chosen to allow for categorization of an asymmetry: orbits, zygoma, ears (external

auditory meatus), maxilla, articular fossa and lower face (including the mandibular body, condyle, and ramus). The position of the anterior nasal spine and genial tubercle were included to show rotation or deviation of either the maxilla or mandible from the mid-sagittal plane (Table 1).

Table 1 Landmark Description: Landmarks which were identified on the oriented three-dimensional volumetric view of the patient.

Landmark	Description
Sella†	*Sella*: Midpoint in sella turcica anterior/posterior, laterally and horizontally
Sella Prime†	*Sella Prime*: Most posterior and medially located point on the posterior wall of sella turcica of the sphenoid bone. Can be used as alternate origin if Sella is not desired
Na†	*Nasion*: Most posterior point on the curvature between the frontal bone and the nasal bone
Or*†	*Orbitale:* Lowest point on the crest of infraorbital rim margin of each orbit
Ba†	*Basion*: Midpoint on the anterior rim of the Foramen Magnum on the occipital bone
Ro*†	*Foramen Rotundum*: The most lateral and inferior portion of the foramen rotundum on the sphenoid bone as viewed from a frontal plane position
Zp*	*Zygonion Point*: Most lateral point on the zygomatic crest where the zygomatic arch is the widest
GlS*	*Glenoid Fossa Superior*: The most superior point of the glenoid fossa of

	the temporal bone
GlA*	*Glenoid Inferior/Articular Eminence*: The most inferior point of the articular eminence of the temporal bone
Cp*	*Condylion Point (Posterioris)*: Most superior and posterior aspect of the condyle
Po*	*Porion (anatomical)*: Highest midpoint on the roof of the entrance to the external auditory meatus
ANS	*Anterior Nasal Spine*: Most anterior point of the nasal floor
Go1*	*Gonion Point 1*: Most posterior point of the posterior border of the ramus of the mandible
Go2*	*Gonion Point 2 (Gonial Notch)*: Most superior point of the of the inferior body of the mandible directly anterior to Gonion.
F/Mental Foramen*	*Mental Foramen*: The most inferior point of the fossa of the mandibular foramen crest
Genial Tubercle	*Genial Tubercle*: Midpoint of the genial tubercle
	*denotes bilateral point †denotes point essential to axis orientation

Midface and Maxillary Region Landmarks

The following figures depict the location of each of the landmarks used to determine asymmetry in the maxilla of the craniofacial skeleton in three different axes (Figures 6-13).

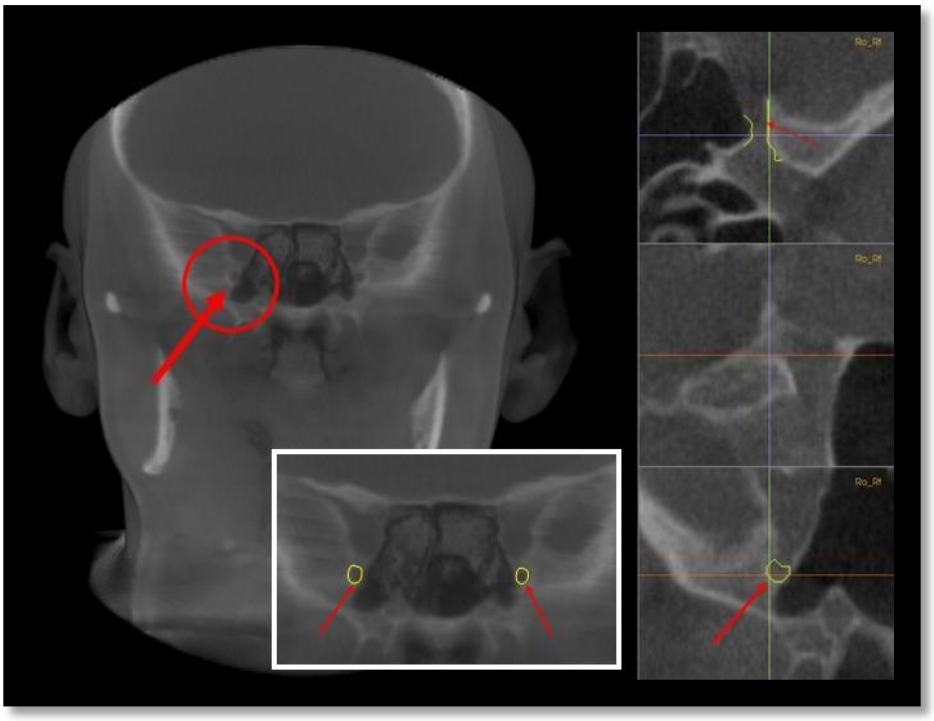

Figure 6 (Foramen Rotundum): ***Ro***, most lateral portion of the foramen rotundum on both right and left locations of patient. Sagitally, the midpoint within the length of canal was estimated.

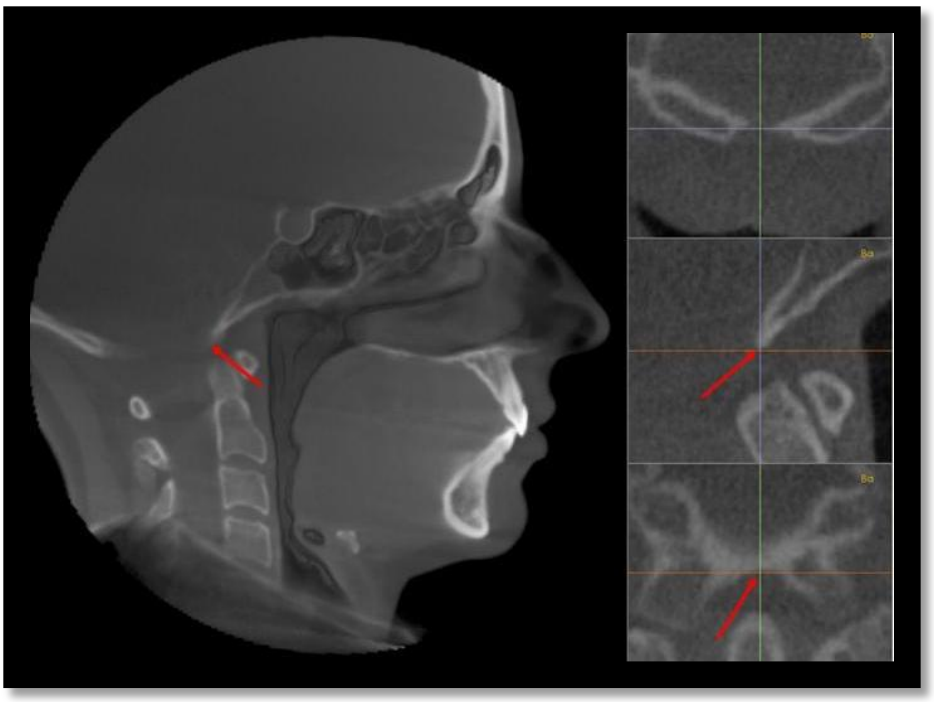

Figure 7 (Basion)*: Ba,* midpoint on anterior rim of the foramen magnum on the occipital bone

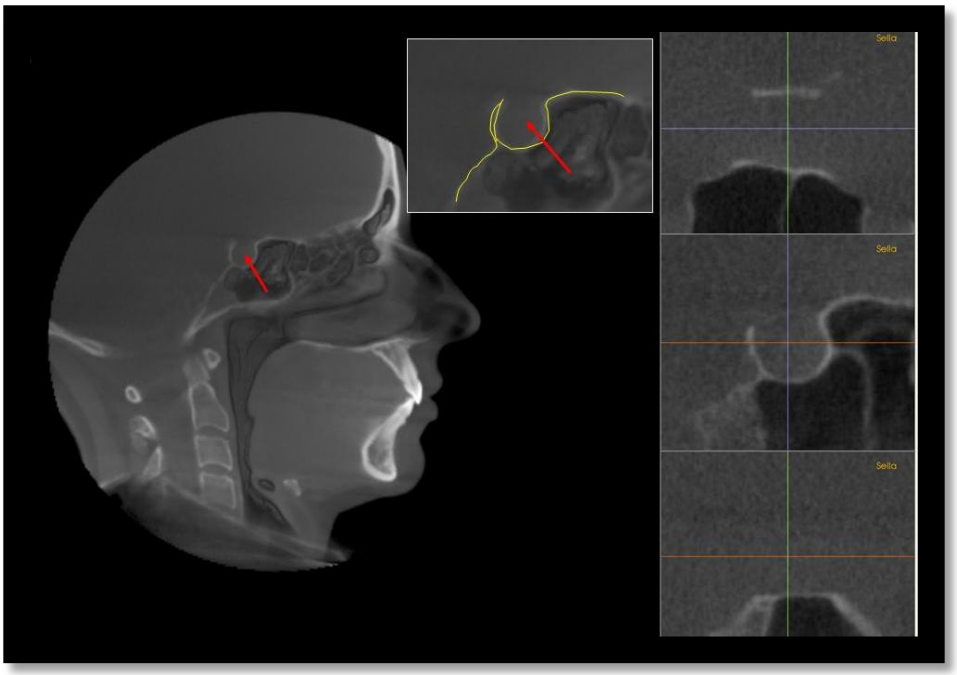

Figure 8 (Sella): *Sella,* midpoint in sella turcica, A-P, laterally and horizontally

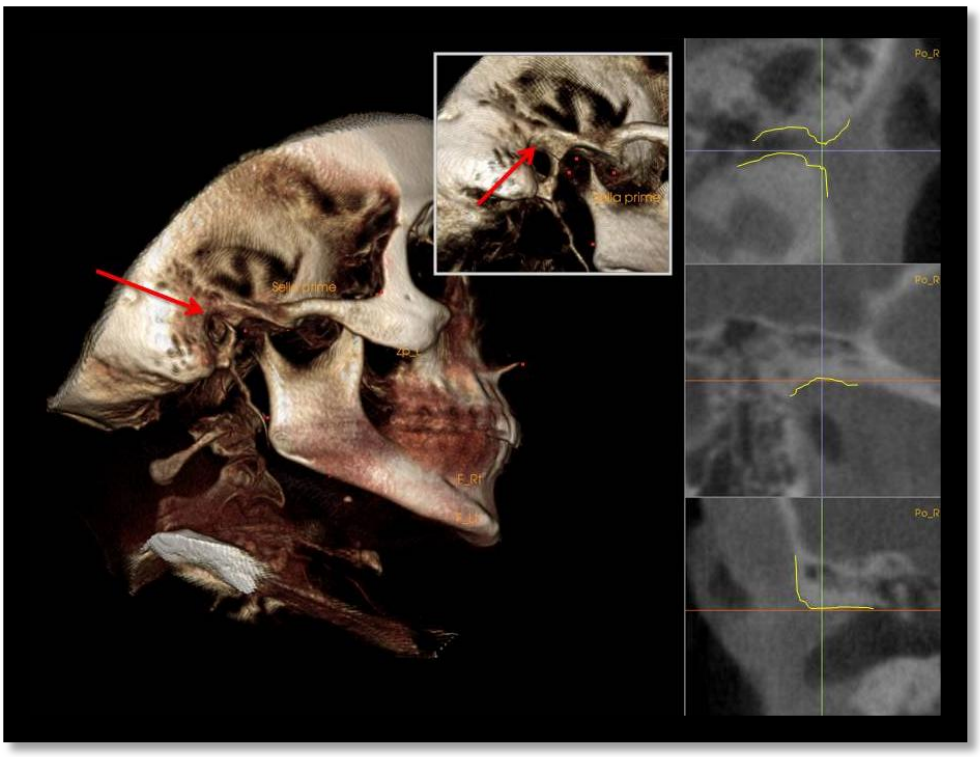

Figure 9 (Anatomical porion): ***Po,*** Highest midpoint on roof of external auditory meatus

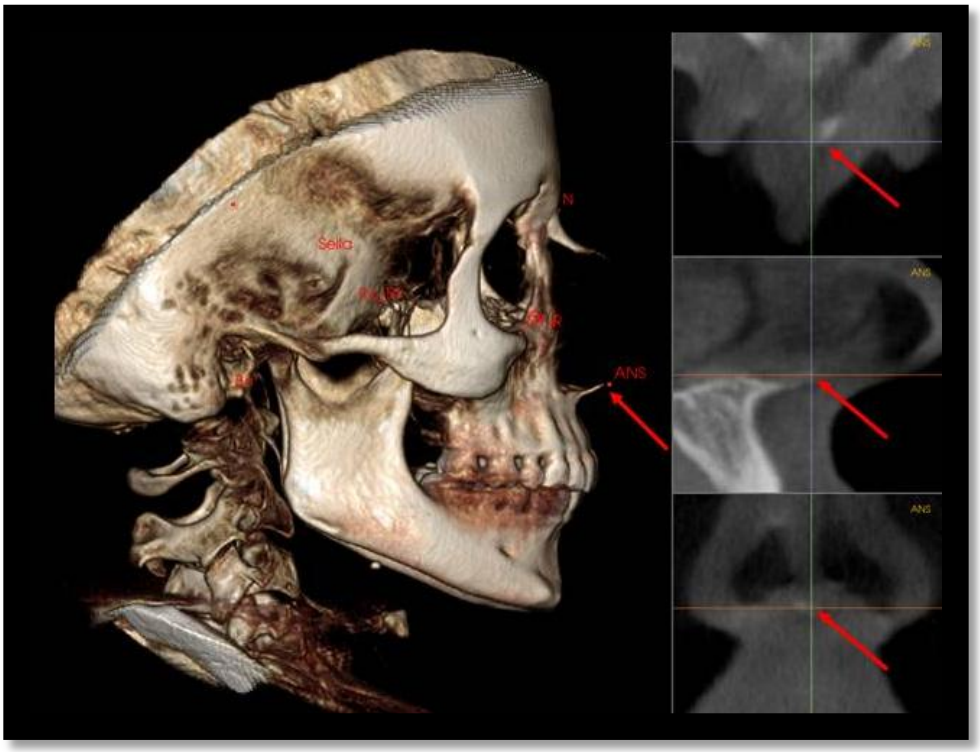

Figure 10 (Anterior Nasal Spine): ***ANS,*** Most anterior point of nasal floor

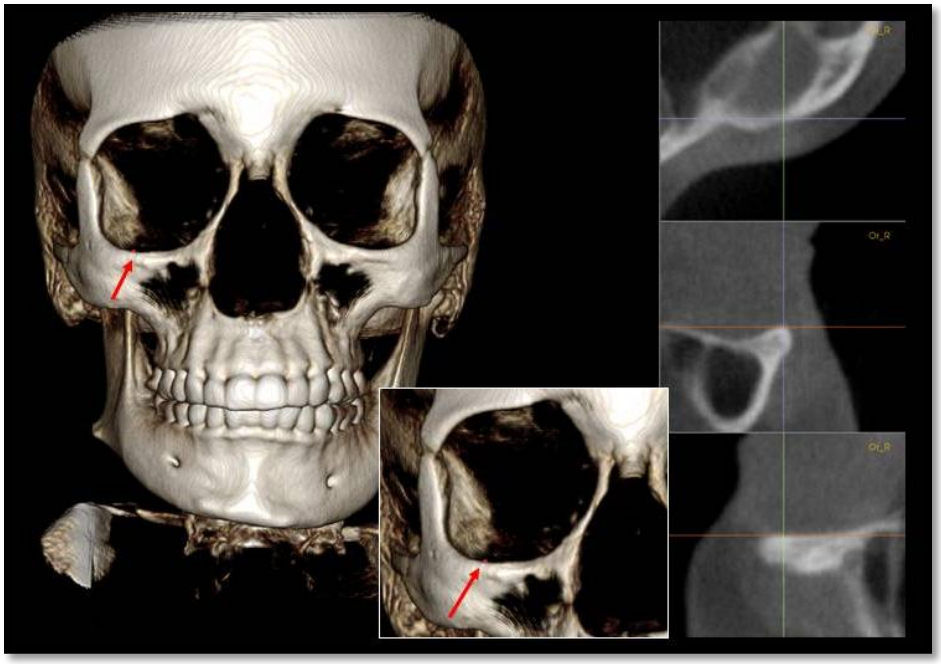

Figure 11 (Orbitale): ***Or*** , Lowest point on infraorbital margin of each orbit

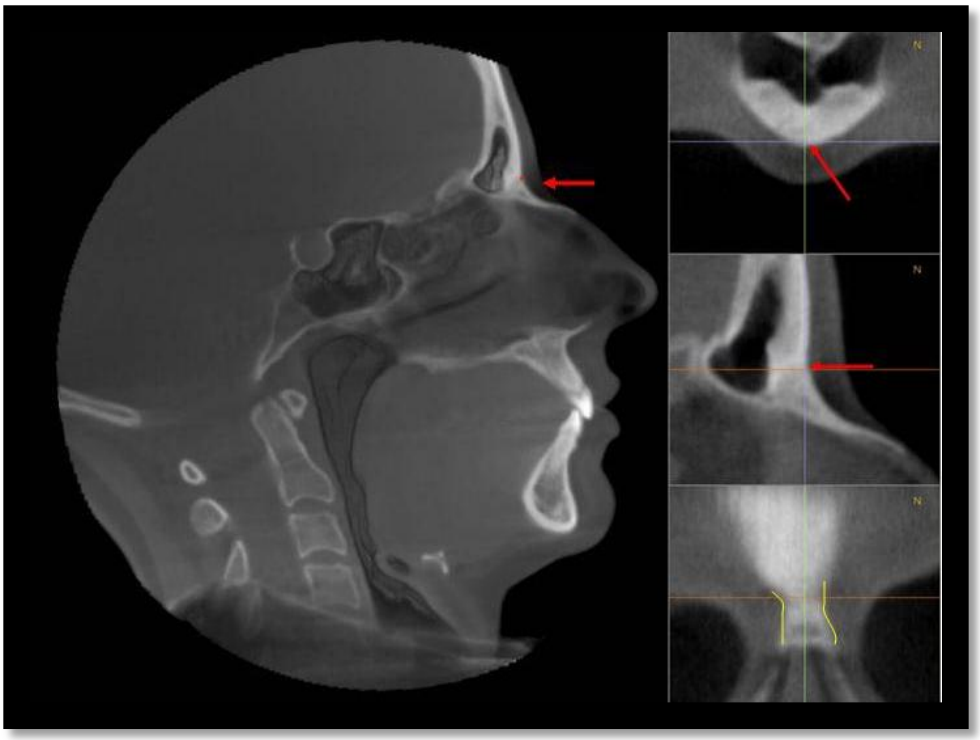

Figure 12 (Nasion): ***Na,*** Most posterior point on curvature between frontal bone and nasal bone in midsagittal plane

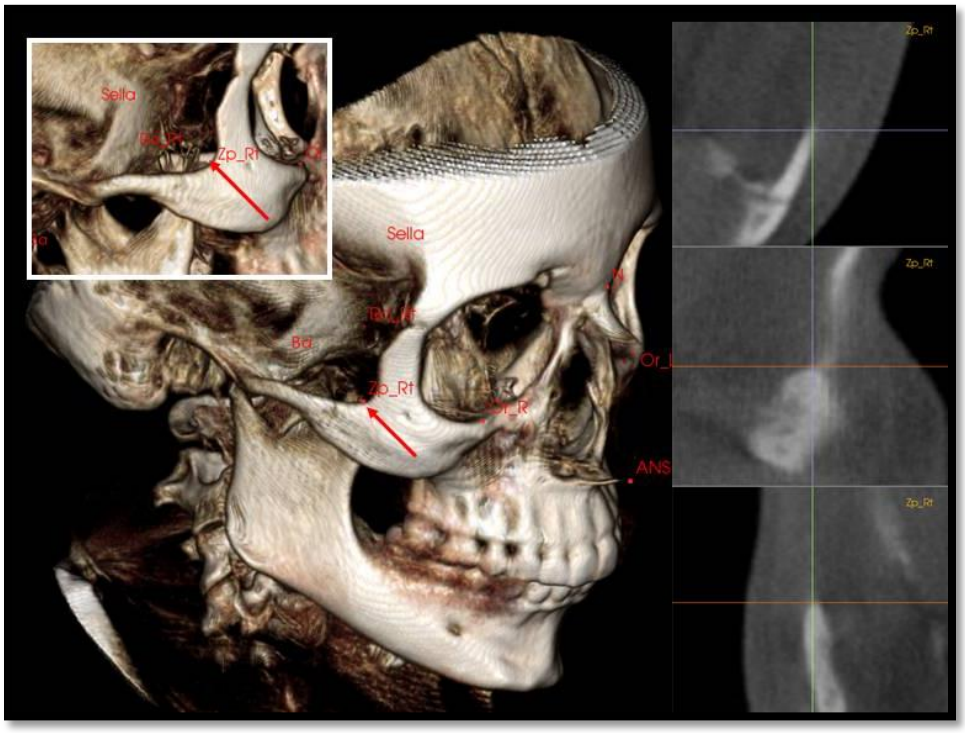

Figure 13 (Zygonion point): ***ZP***, Most lateral point where zygomatic arch is widest

Mandibular Region Landmarks

The following figures depict the location of each of the landmarks used to determine asymmetry in the mandible of the craniofacial skeleton in three different axes (Figures 14-18).

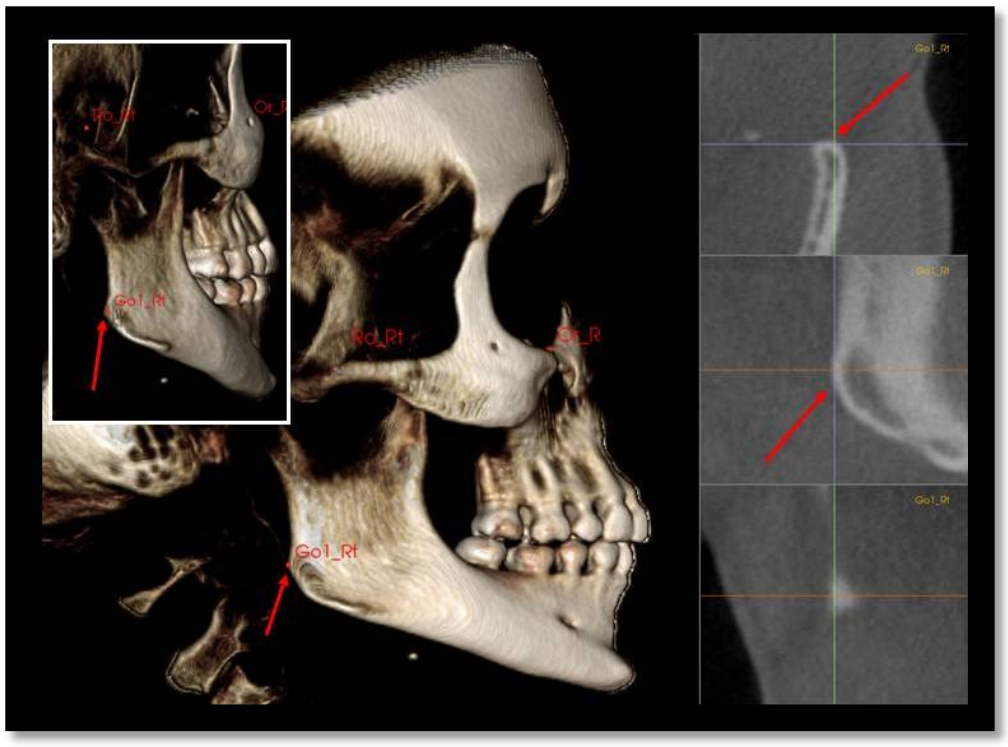

Figure 14 (Gonion 1): ***Go1***, Most posterior point of posterior border of ramus

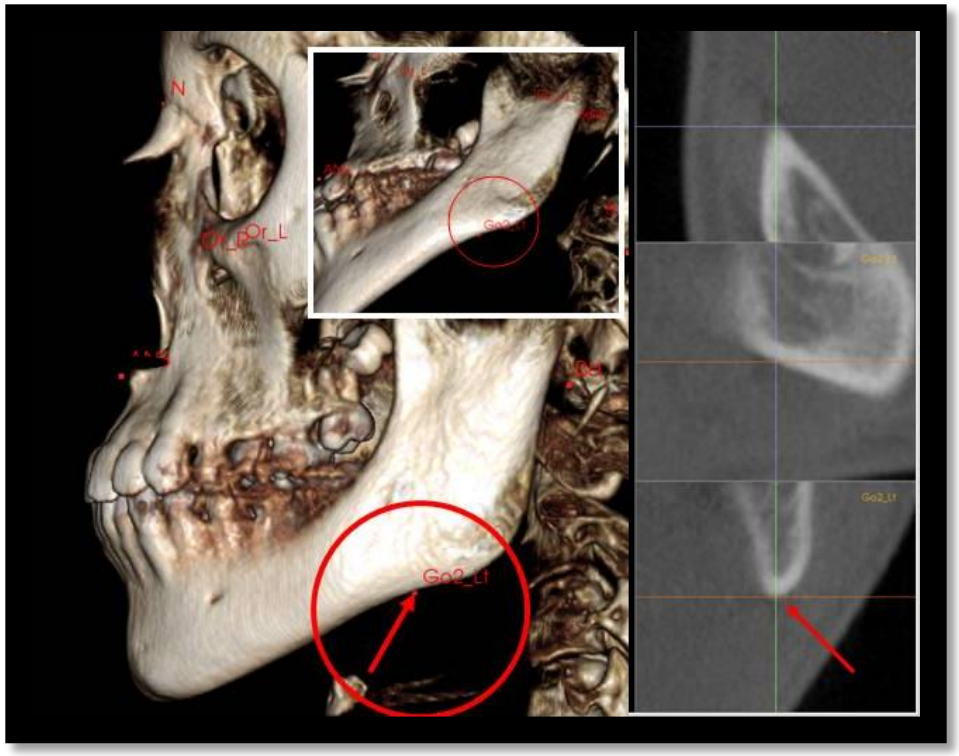

Figure 15 (Gonion 2): **Go2**, Most inferior point of posterior border of ramus

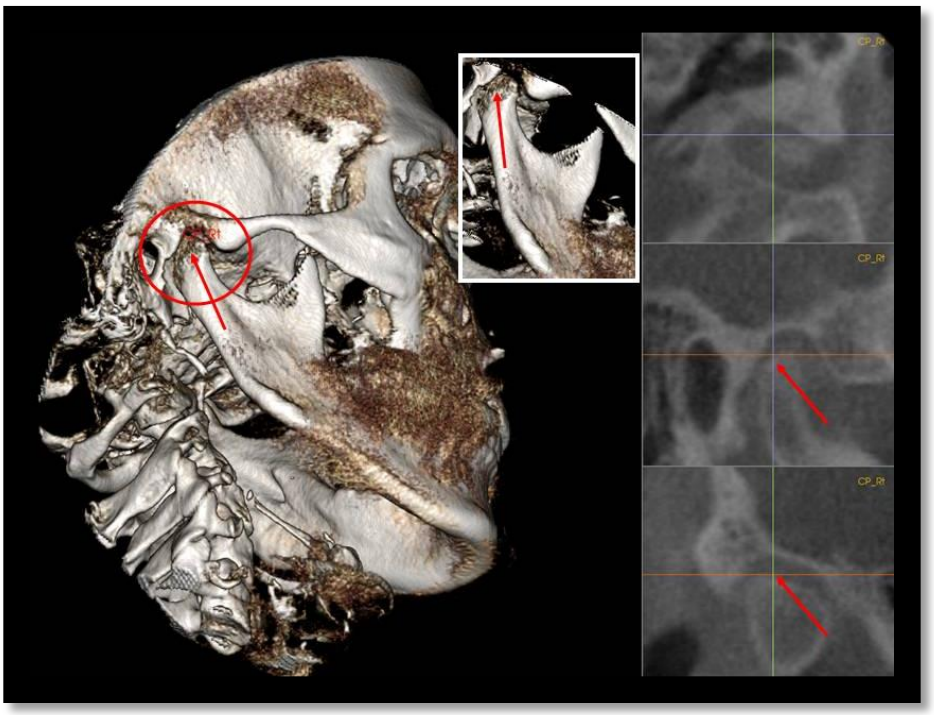

Figure 16 (Condylion posterioris): ***CP,*** Most superior and posterior aspect of condyle

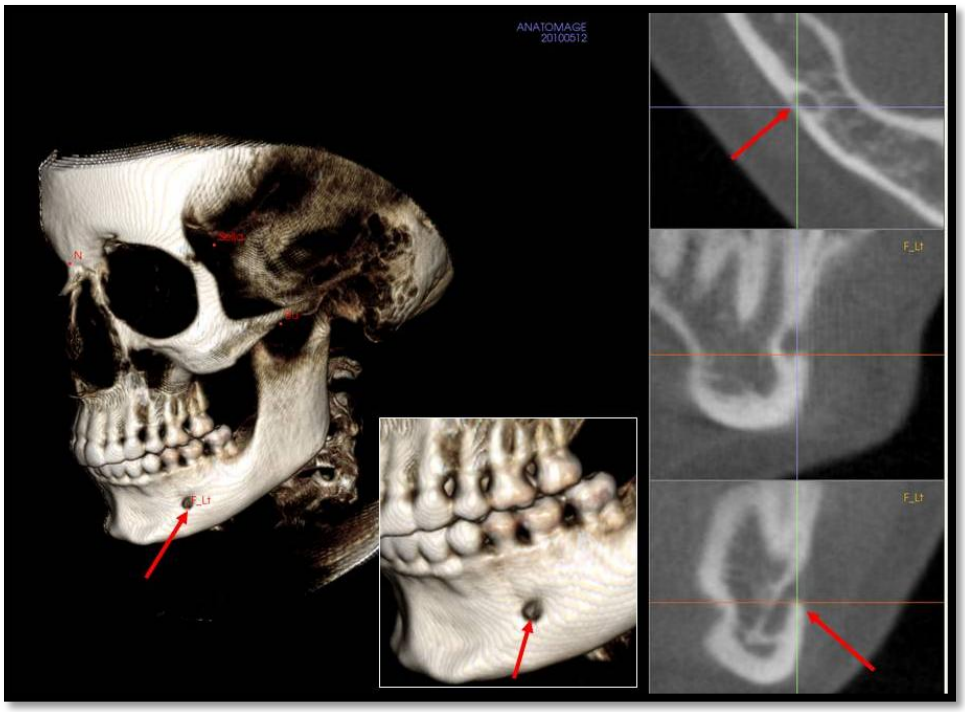

Figure 17 (Mental foramen): ***F***, The most inferior portion of the fossa of the Md foramen (or MF if using the center of the mental foramen)

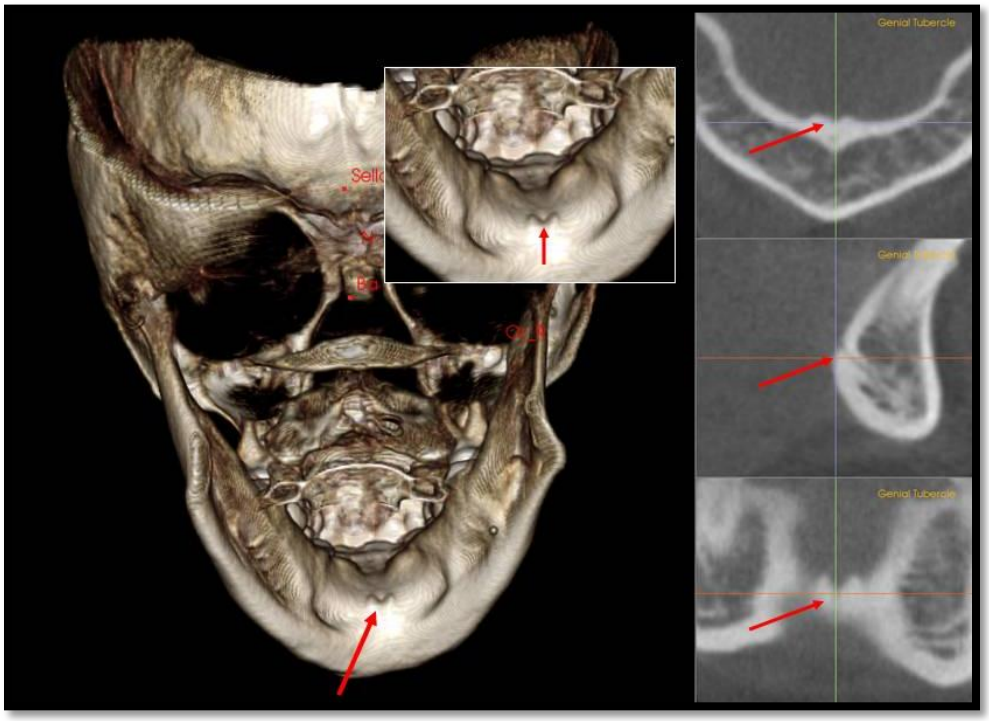

Figure 18 (Genial Tubercle): ***G,*** Midpoint of the genial tubercle

Temporal Region Landmarks

The following figures depict the location of each of the landmarks used to determine asymmetry in the mandibular fossa and articular eminence of the craniofacial skeleton in three different axes (Figures 19-21).

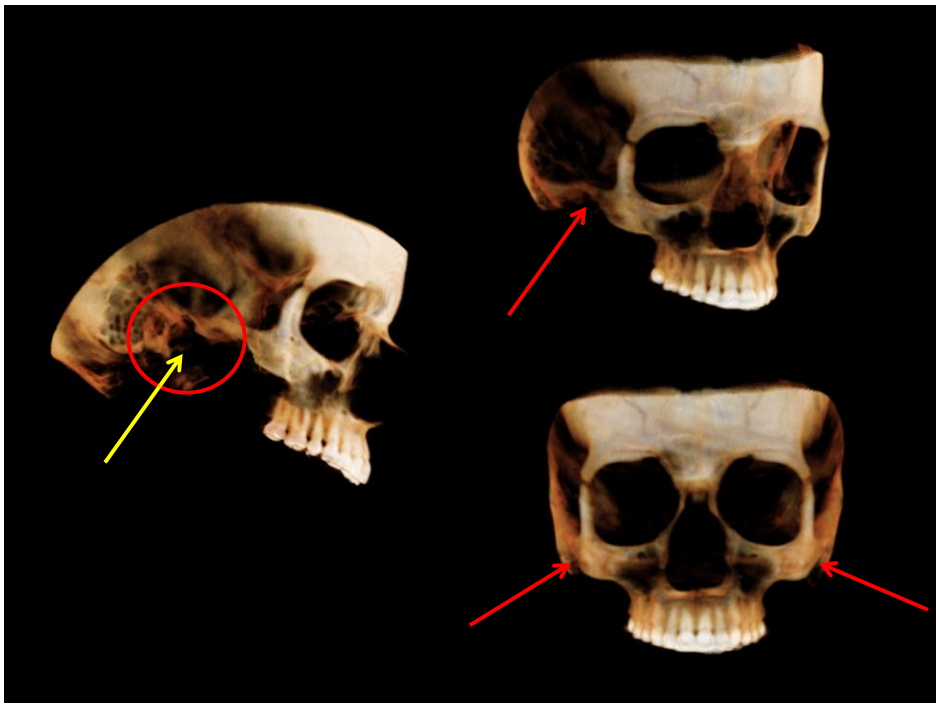

Figure 19 (Temporal Region): Area of the glenoid fossa and articular eminence shown in three dimensional views

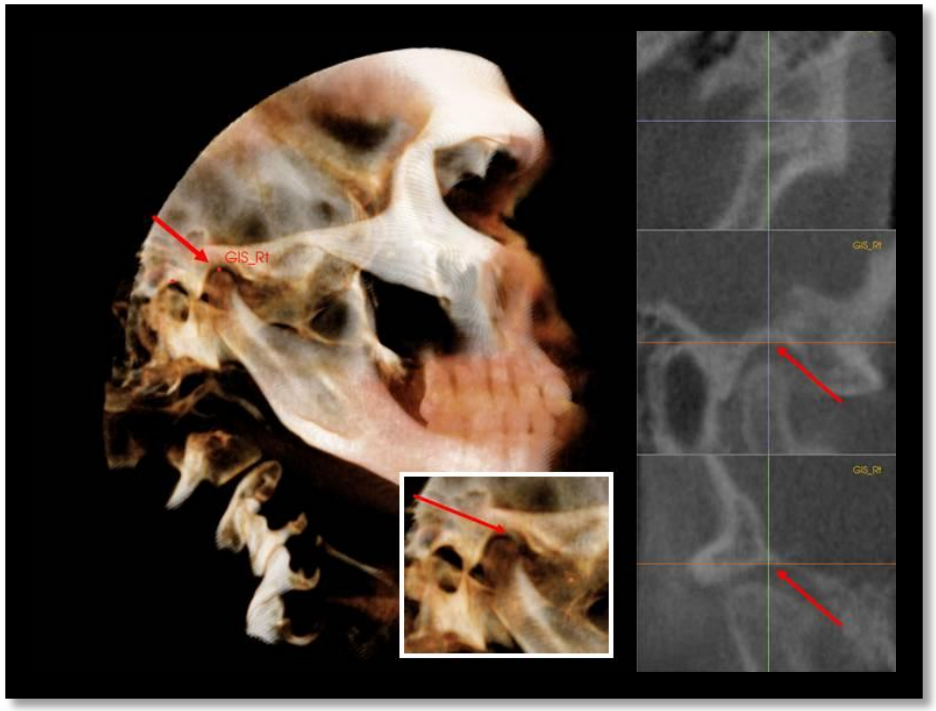

Figure 20 (Glenoid Superior): ***GlSR and GlSL,*** The most superior point of the glenoid fossa of the temporal bone

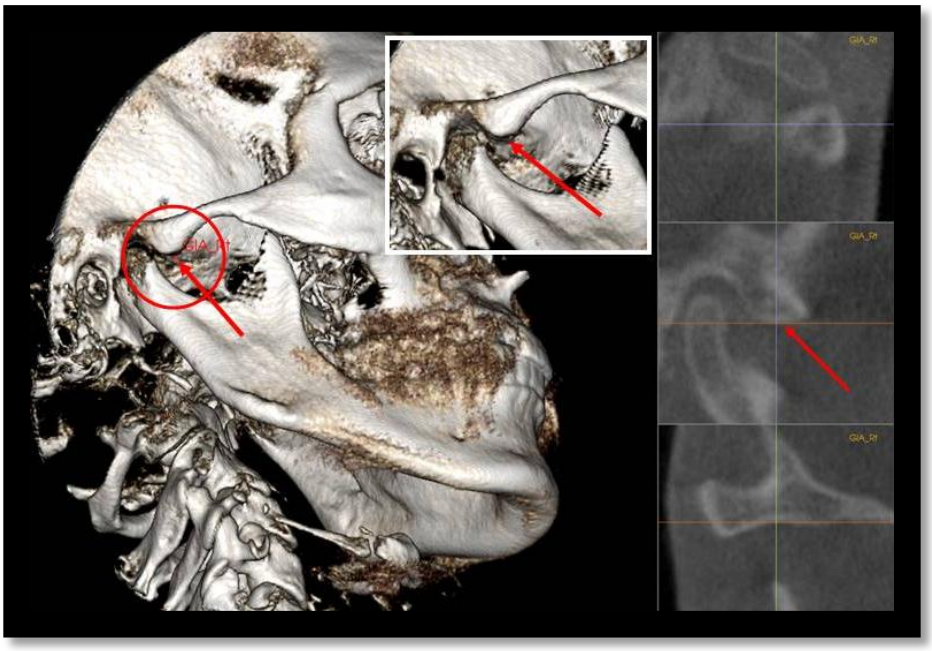

Figure 21 (Glenoid/Articular Eminence): ***GlAR and GlAL,*** The most inferior point of the articular eminence of the temporal bone

Constructing the Analysis Measurements

In order to construct an analysis of measurements based on the set of landmarks and axis that had been identified, each parameter of measurement had to be constructed and the measurement named. In order to combine the measurements together for easy visualization, a new group had to be constructed. Under settings, the "Group" tab was selected, and "Add" was selected at the lower left hand corner of the menu (Figure 22).

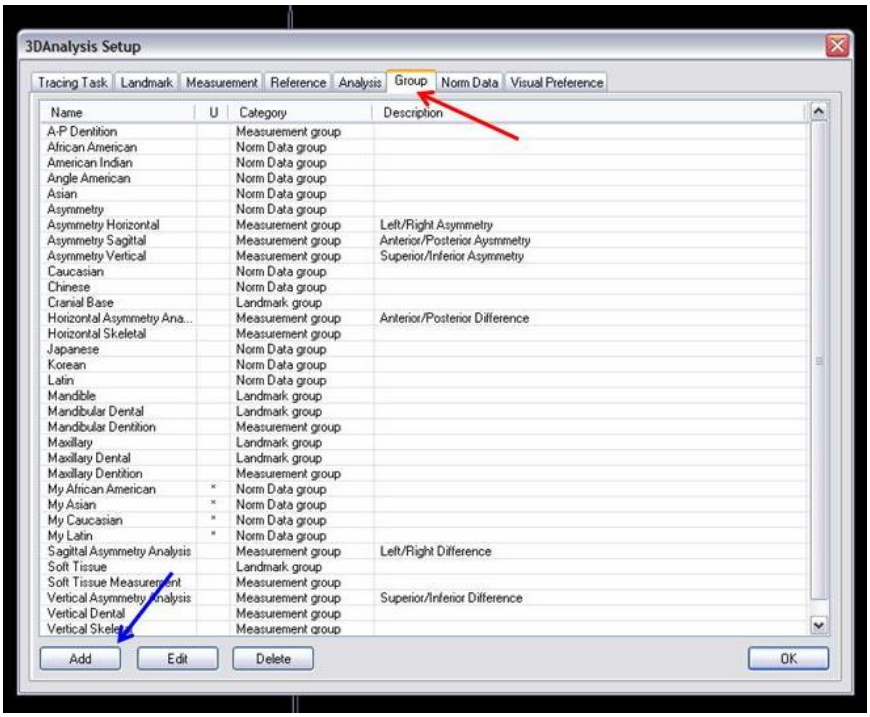

Figure 22: Example of the software page illustrating the "Group" tab that allows for additional categories of measurements to be defined.

A new menu appeared that allowed the naming of this new grouping of points (Asymmetry Horizontal, Figure 23) and defined how each investigator would categorize this group. Since the investigator was making a new group for measurements, the selection for "measurement grouping" was highlighted and "ok" was selected to create this new group. This was repeated for "Asymmetry Vertical" and "Asymmetry Sagittal" considering the measurements were defined in all three dimensions. All groups had to be created prior to defining the parameters for each measurement.

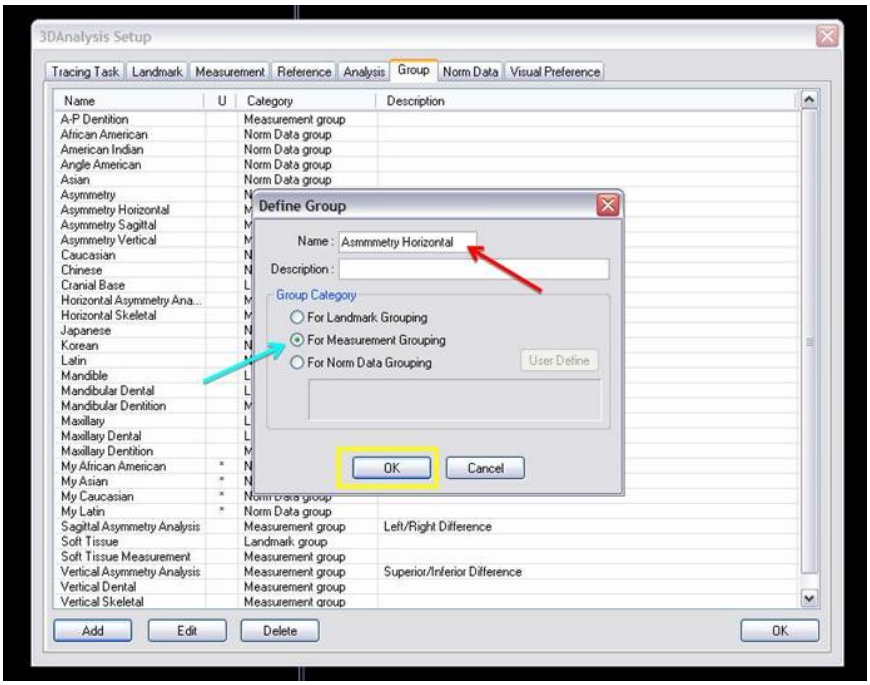

Figure 23: Example of the Anatomage InVivo window illustrating the defining of the group name as Asymmetrical Horizontal and selecting the proper "Group Category".

Once each Group had been defined, the proper parameters for each measurement were established. Having the majority of measurements made from a landmark to one of the three origin planes, it allowed the investigator to separate right/left, superior/inferior, and anterior/posterior in terms of orientation of each landmark. This permitted identification of bilateral structures and their orientation to their ipsilateral counterpart.

Under the "Measurement" tab in "Settings", the "Add" tab was selected to begin the process of defining of each parameter (Figure 24).

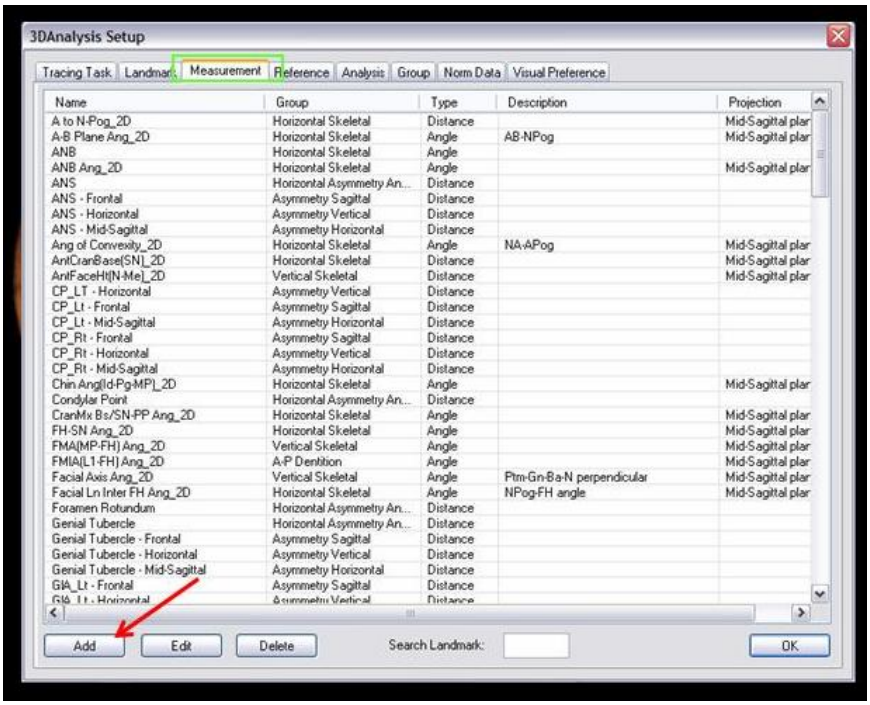

Figure 24: View of one software page listing measurements and the position of the ADD choice to define each parameter.

A new window opens so the investigator can construct each parameter of each measurement in each of the three dimensions. An example is shown using the landmark and measurement of Orbitale Right (Figures 25-28).

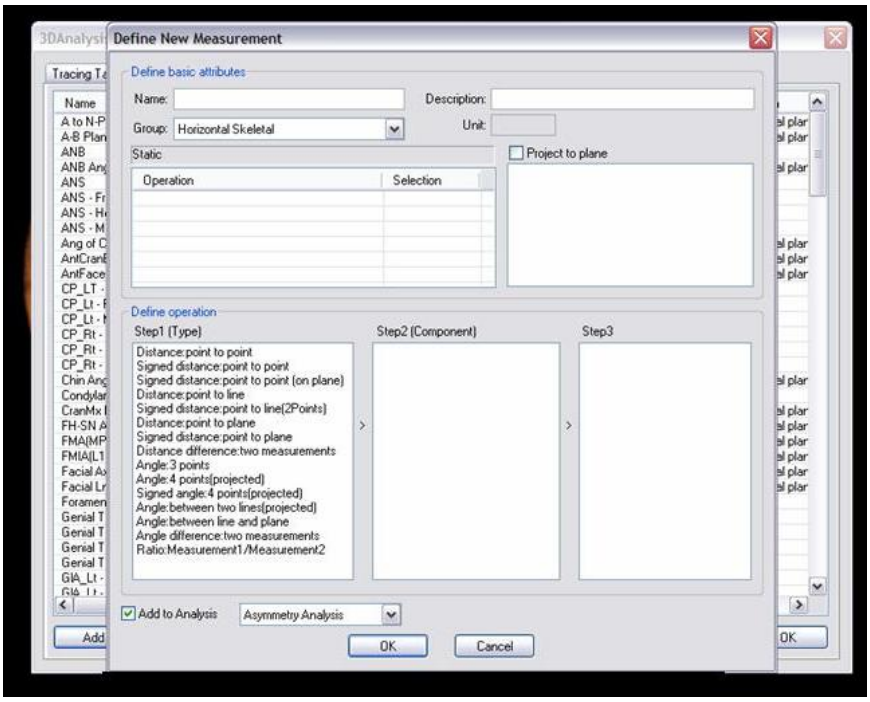

Figure 25: View of software page in which the new measurement could be defined.

Once the "Define New Measurement" window was opened (Figure 25), the name of a measurement was affixed, in this case, Orbitale Right to the Mid-Sagittal Plane is the example.

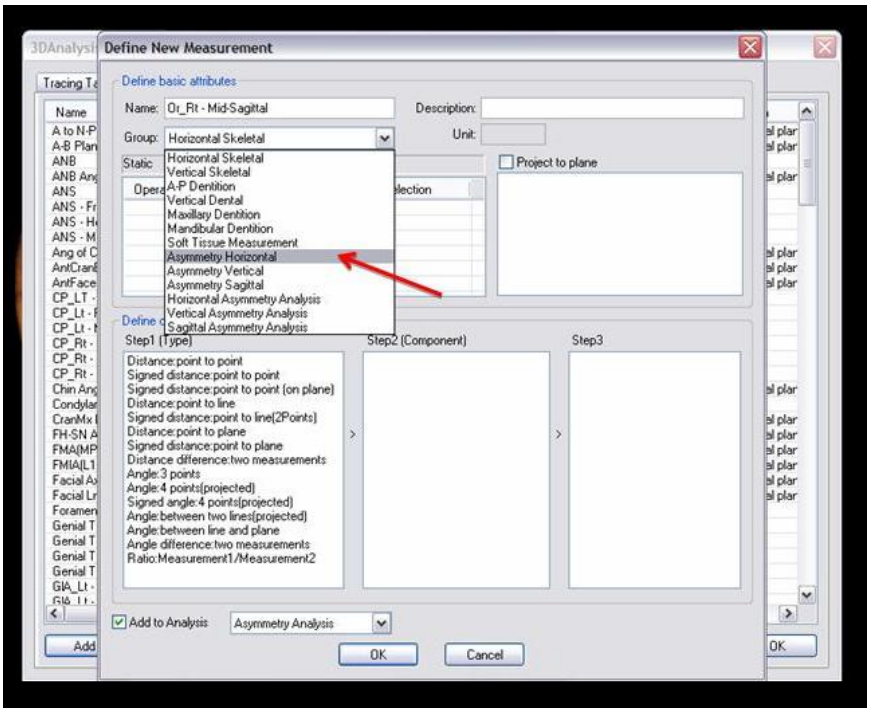

Figure 26: View of software page showing the subroutine to define a new measurement and applying it to a group.

The "Group" must then be assigned. If the measurement was to the mid-sagittal plane, this would be considered a horizontal measurement and assigned to the "Asymmetry Horizontal" grouping in the pull down menu (Figure 26). This process must be repeated for all points outside of the origin points for the specified points (Sella, Nasion, and Basion).

Once the measurement had been labeled and grouped, its parameters were defined. Since the axes are labeled positive and negative, the measurements could be measured in either a "signed distance: point to plane" or simply "distance point to plane" (Figure 27). If the measurement was not "signed" (labeled as positive or negative), it made little difference except if the investigator wished to subtract ipsilateral landmark values (which will be described later in this text).

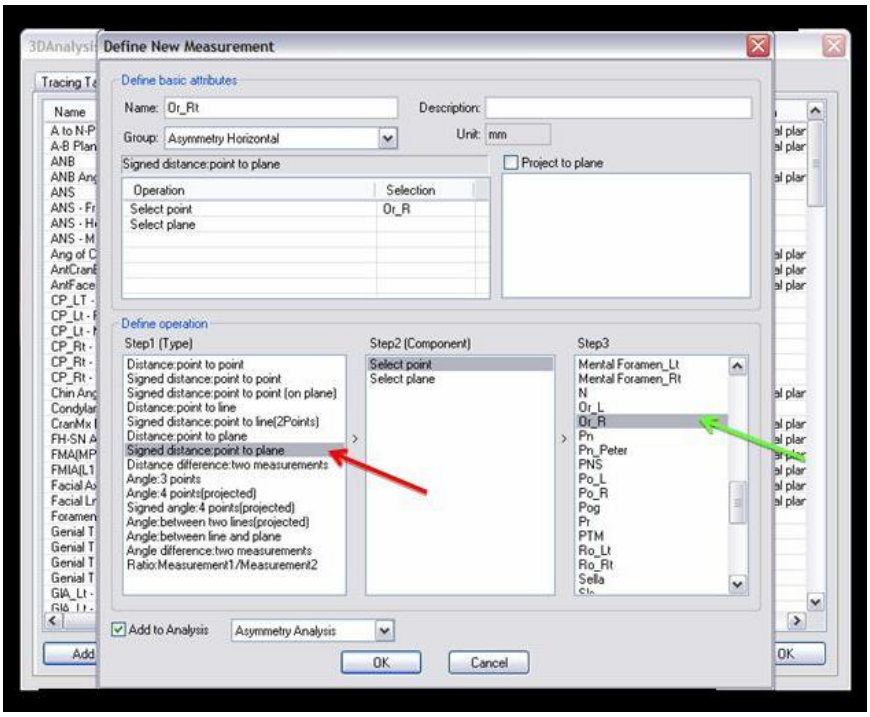

Figure 27: View of the software page showing how to assign a new measurement. Selection of the type of measurement is shown by the red arrow and the point which the measurement will based from. For this example, Orbitale Right is serving as the measured point.

The "select point" was chosen under the Step 2 (Component) portion of the middle menu, and the proper point was located on the right hand scroll down menu. Following point selection, the investigator selected the plane in the same manner by selecting "Select plane" from the Step 2 (Component) menu and locating the proper plane, in our example, the Mid-Sagittal plane (Figure 28).

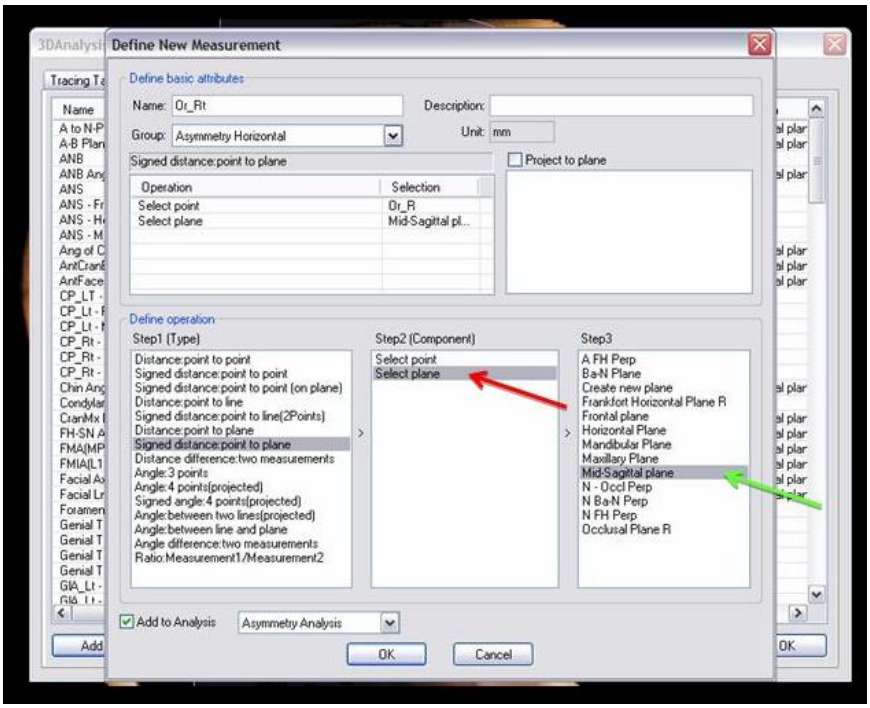

Figure 28: View of software page indicating the second and third steps in the process under the Step 2 Component. The plane will serve as the measurement origin with the previous selected point being the measured mark. In this example, the plane in which the measurement is taken from is the Mid-Sagittal Plane.

This process was repeated for all landmarks as measured for each of the respective x,y,z planes and grouped accordingly (*i.e.*, those points measured to the frontal plane were sagittal measurements and grouped under Asymmetry Sagittal; Figure 29). Once all landmark measurements had been compiled, a summary of measurements were found under the Measurement tab and arranged according to their group by simply clicking on the "Group" category heading.

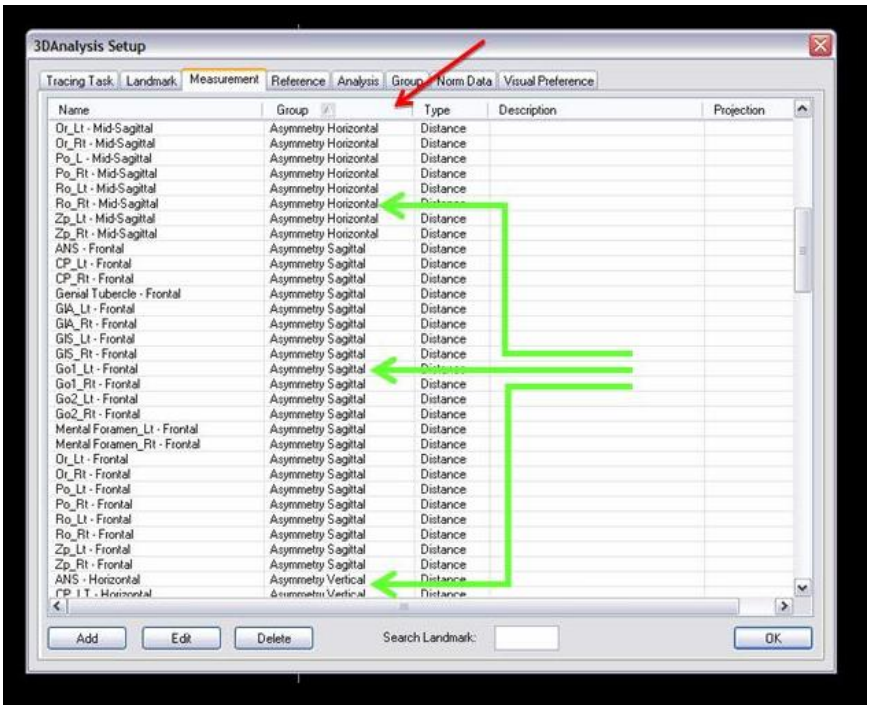

Figure 29: View of "Measurement" software page showing each "Group" of measurements for given perspective (either Sagittal, Horizontal or Vertical).

After all measurements had been established, an analysis was constructed that summarized all the data that had been measured. By selecting the "Analysis" tab under "settings", the investigator added a user-defined analysis (Figure 30).

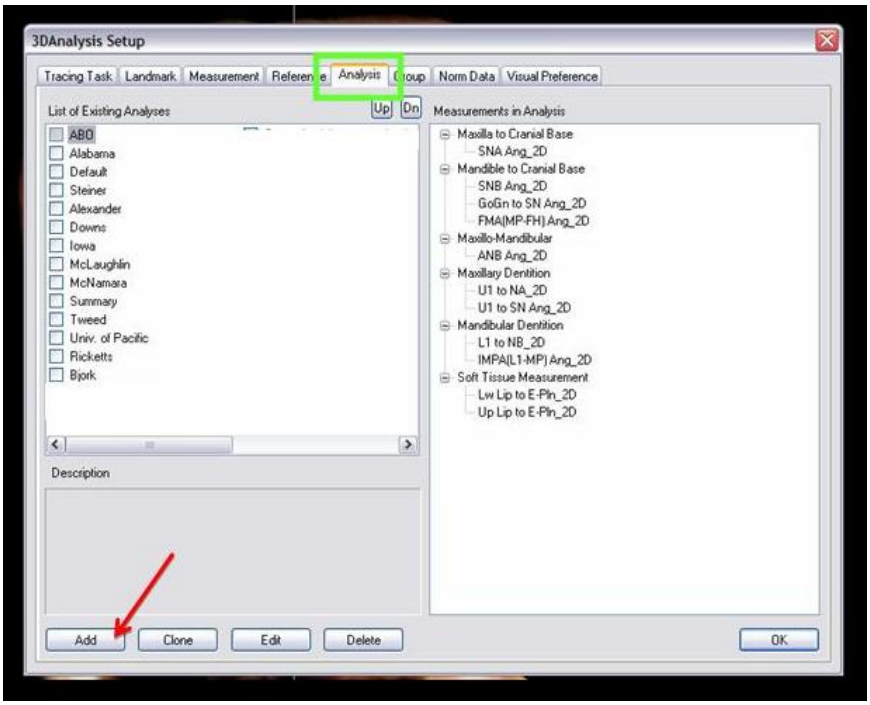

Figure 30: A view of a software page indicating the subroutine adding a customized analysis under the "Analysis" tab in the 3DAnalysis Setup menu

The name of the analysis had to be entered, which, in this case, is the "Asymmetry Analysis". Scrolling down the menu on the right hand side allowed the investigator to see all existing measurements that had been defined (Figure 31). The investigator then began selecting the "Asymmetry Horizontal" grouping of points and moving the entire group to the Asymmetry Analysis by clicking the left pointing arrow, thereby shifting all measurements in that grouping to the defined analysis (Figure 31).

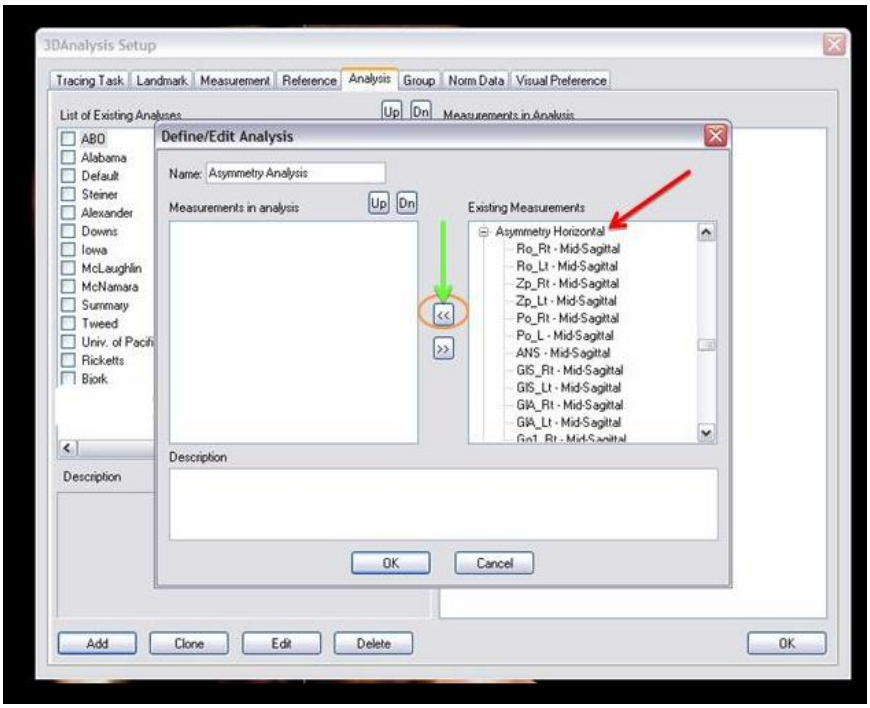

Figure 31: A view of software page demonstrating the process through which existing measurements under the "Asymmetry Horizontal" group of measurements are moved to the newly created "Aymmetry Analysis."

This process was then repeated for the "Asymmetry Vertical" and "Asymmetry Sagittal" groupings, completing the measurement portion of the analysis (Figure 32).

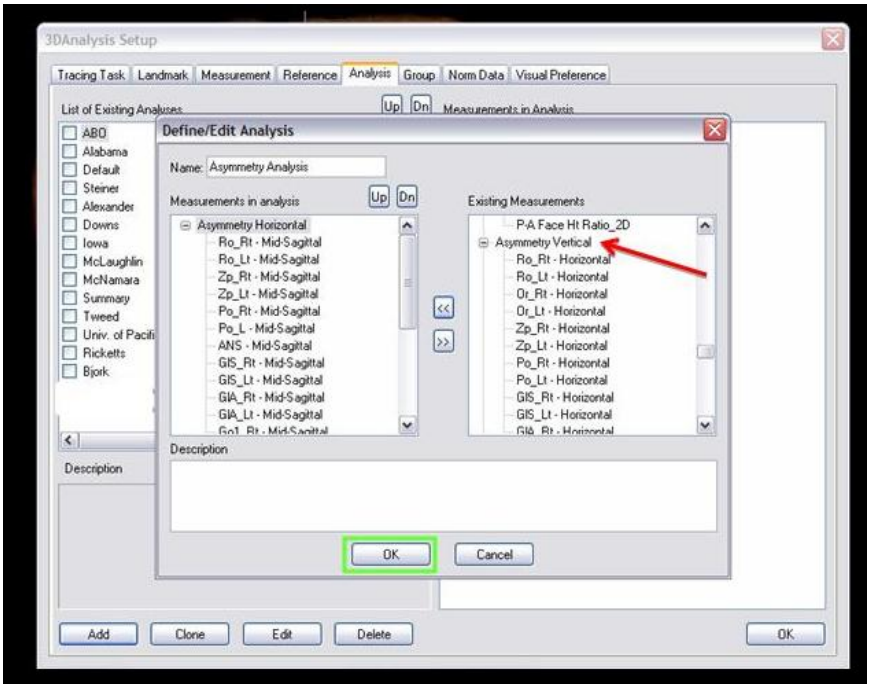

Figure 32: A view of the software indicating both the list of the measurements used in one group, Asymmetry Horizontal (left), and the potential measurements that could be used (right).

After the user-defined analysis was completed, it appeared under the "Analysis" tab under settings (Figure 33). By selecting this analysis, the investigator returned to the 3D Analysis module and viewed all measurements (Tables 2-4).

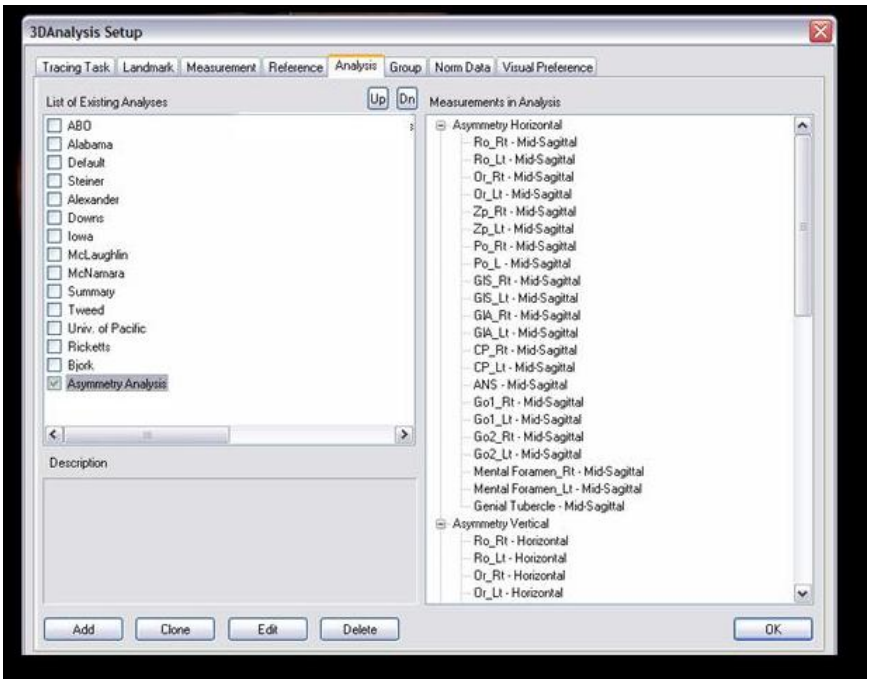

Figure 33: A view of software indicating several types of analyses (left) with the created "Aymmetry Analysis" highlighted, and the type of measurements in that analysis (right).

Table 2 Mid-Sagittal Plane Measurments: Measurements derived from landmark location perpendicular to the Mid-sagittal plane

Measurement	Description
Ro_Rt – Mid-Sagittal	Right Foramen Rotundum to Mid-Sagittal Plane
Ro_Lt – Mid-Sagittal	Left Foramen Rotundum to Mid-Sagittal Plane
Zp_Rt – Mid-Sagittal	Right Zigonion Point to to Mid-Sagittal Plane
Zp_Lt – Mid-Sagittal	Left Zigonion Point to Mid-Sagittal Plane
Po_Rt – Mid-Sagittal	Right Porion to Mid-Sagittal Plane
Po_Lt – Mid-Sagittal	Left Porion to Mid-Sagittal Plane
GlS_Rt – Mid-Sagittal	Superior point of the Right Gleniod Fossa to Mid-Sagittal Plane
GlS_Lt – Mid-Sagittal	Superior point of the Left Gleniod Fossa to Mid-

	Sagittal Plane
GlA_Rt – Mid-Sagittal	Inferior portion of the Right Articular Eminence to Mid-Sagittal Plane
GlA_Lt – Mid-Sagittal	Inferior portion of the Left Articular Eminence to Mid-Sagittal Plane
Cp_Rt – Mid-Sagittal	Right Condyle Point to Mid-Sagittal Plane
Cp_Lt – Mid-Sagittal	Left Condyle Point to Mid-Sagittal Plane
ANS – Mid-Sagittal	Anterior Nasal Spine to Mid-Sagittal Plane
Go1_Rt – Mid-Sagittal	Right Gonial Point to Mid-Sagittal Plane
Go1_Lt – Mid-Sagittal	Left Gonial Point to Mid-Sagittal Plane
Go2_Rt – Mid-Sagittal	Right Gonial Notch to Mid-Sagittal Plane
Go2_Lt – Mid-Sagittal	Left Gonial Notch to Mid-Sagittal Plane
Ment. Foramen_Rt – Mid-Sagittal	Right Mental Foramen to Mid-Sagittal Plane
Ment. Foramen_Lt – Mid-Sagittal	Left Mental Foramen to Mid-Sagittal Plane
Genial Tubercle – Mid-Sagittal	Genial Tubercle to Mid-Sagittal Plane

Table 3 Horizontal Plane Measurements: Measurements derived from landmarks perpendicular to the Horizontal plane

Measurement	Description
Ro_Rt – Horizontal	Right Foramen Rotundum to Horizontal Plane
Ro_Lt – Horizontal	Left Foramen Rotundum to Horizontal Plane
Zp_Rt – Horizontal	Right Zigonion Point to to Horizontal Plane
Zp_Lt – Horizontal	Left Zigonion Point to Horizontal Plane
Po_Rt – Horizontal	Right Porion to Horizontal Plane
Po_Lt – Horizontal	Left Porion to Horizontal Plane
GlS_Rt – Horizontal	Superior point of the Right Gleniod Fossa to Horizontal Plane
GlS_Lt – Horizontal	Superior point of the Left Gleniod Fossa to Horizontal Plane
GlA_Rt – Horizontal	Inferior portion of the Right Articular Eminence to Horizontal Plane
GlA_Lt – Horizontal	Inferior portion of the Left Articular Eminence to Horizontal Plane
Cp_Rt – Horizontal	Right Condyle Point to Horizontal Plane
Cp_Lt – Horizontal	Left Condyle Point to Horizontal Plane
ANS – Horizontal	Anterior Nasal Spine to Horizontal Plane
Go1_Rt – Horizontal	Right Gonial Point to Horizontal Plane
Go1_Lt – Horizontal	Left Gonial Point to Horizontal Plane
Go2_Rt – Horizontal	Right Gonial Notch to Horizontal Plane
Go2_Lt – Horizontal	Left Gonial Notch to Horizontal Plane
Ment. Foramen_Rt – Horizontal	Right Mental Foramen to Horizontal Plane
Ment. Foramen_Lt – Horizontal	Left Mental Foramen to Horizontal Plane
Genial Tubercle – Horizontal	Genial Tubercle to Horizontal Plane

Table 4 Frontal/Coronal Plane Measurements: Measurements derived from landmarks perpendicular to Frontal plane.

Measurement	Description
Ro_Rt – Frontal	Right Foramen Rotundum to Frontal Plane
Ro_Lt – Frontal	Left Foramen Rotundum to Frontal Plane
Zp_Rt – Frontal	Right Zigonion Point to to Frontal Plane
Zp_Lt – Frontal	Left Zigonion Point to Frontal Plane
Po_Rt – Frontal	Right Porion to Frontal Plane
Po_Lt – Frontal	Left Porion to Frontal Plane
GlS_Rt – Frontal	Superior point of the Right Gleniod Fossa to Frontal Plane
GlS_Lt – Frontal	Superior point of the Left Gleniod Fossa to Frontal Plane
GlA_Rt – Frontal	Inferior portion of the Right Articular Eminence to Frontal Plane
GlA_Lt – Frontal	Inferior portion of the Left Articular Eminence to Frontal Plane
Cp_Rt – Frontal	Right Condyle Point to Frontal Plane
Cp_Lt – Frontal	Left Condyle Point to Frontal Plane
ANS – Frontal	Anterior Nasal Spine to Frontal Plane
Go1_Rt – Frontal	Right Gonial Point to Frontal Plane
Go1_Lt – Frontal	Left Gonial Point to Frontal Plane
Go2_Rt – Frontal	Right Gonial Notch to Frontal Plane

Go2_Lt – Frontal	Left Gonial Notch to Frontal Plane
Ment. Foramen_Rt – Frontal	Right Mental Foramen to Frontal Plane
Ment. Foramen_Lt – Frontal	Left Mental Foramen to Frontal Plane
Genial Tubercle – Frontal	Genial Tubercle to Frontal Plane

Defining Overlay Wiggle-Gram

Once all initial landmark measurements had been entered into the analysis, new measurements were defined that allowed the investigator to summarize all the previous findings on both a visual and numerical scale. This new form summarizing the data essentially is a subtractive analysis that compares the left side of the patient against the right. Organizing the data in such a way aids in describing bilateral incongruences between landmarks, thus allowing numerical description of asymmetry for a given landmark to a specific plane. The set of new "Groups" had to be defined in order to properly organize the summarizing data (the same process as previously described to construct our initial "Groups" of measurements). The new groups were named "Horizontal Asymmetry Analysis, Vertical Asymmetry Analysis, and Sagittal Asymmetry Analysis."

One more group was created to allow the construction of an overlay line graph defined as a "wigglegram", and named "Asymmetry" (Figure 34). One difference was that instead of using "For Measurement Grouping," the investigator defined

for “Norm Data Grouping” when adding an additional group. A summary of the new groups can be seen highlighted in Figure 34.

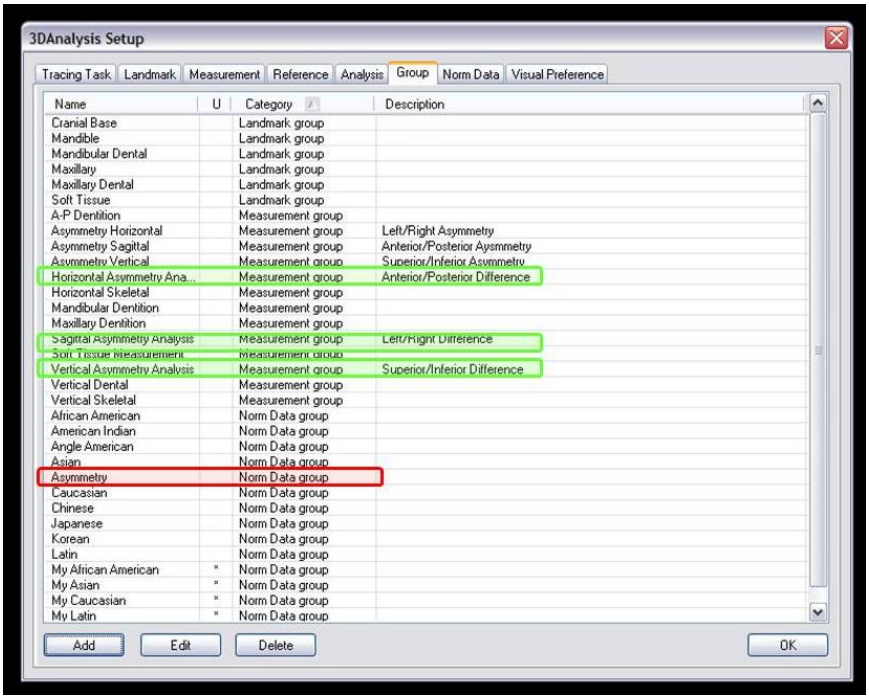

Figure 34: A view of the software showing the four newly defined groups.

Once all additional groups had been correctly added, new measurements were once again added to each group to finish the summarization of the data. The following measurements were used (Table 5).

Table 5 Defining Wiggle-Gram Measurements: List of measurements in three planes (landmark to horizontal plane is used in the description for example only, landmark to coronal/frontal plane and to mid-sagittal plane can be substituted to give all three planes). The final result is a linear description of asymmetry in all three dimensions.

Measurement	Description
Ro	Left Foramen Rotundum to Horizontal Plane value minus Right Foramen Rotundum to Horizontal Plane value
Zp	Left Zygonion Point to Horizontal Plane value minus Right Zygonion Point to to Horizontal Plane value
Po	Left Porion to Horizontal Plane value minus Right Porion to Horizontal Plane value
GlS	Left GlS to Horizontal Plane value minus Right GlS to Horizontal Plane value
GlA	Left GlA to Horizontal Plane value minus Right GlA to Horizontal Plane value
Cp	Left Condyle Point to Horizontal Plane value minus Right Condyle Point to Horizontal Plane value
ANS*	Anterior Nasal Spine to Horizontal Plane (signed value)
Go1	Left Gonial Point to Horizontal Plane value minus Right Gonial Point to Horizontal Plane value
Go2	Left Gonial Notch to Horizontal Plane value minus Right Gonial Notch to Horizontal Plane
Ment. Foramen	Left Mental Forament to Horizontal Plane to Right Mental Foramen to Horizontal Plane
Genial Tubercle*	Genial Tubercle to Horizontal Plane (signed value)
	*indicates values only applicable to horizontal analysis

Statistical Analysis

In order to more accurately determine the reproducibility of all landmarks for each patient, a centroid for each cephalometric point was constructed from the three timepoint tracings using the formula ($C_x=(X_1+X_2+X_3)/3$, $C_y=(Y_1+Y_2+Y_3)/3$, $C_z=(Z_1+Z_2+Z_3)/3$). The use of a centroid reduced the influence that one mistraced cephalometric landmark would have on the remaining two timepoints. A centroid was calculated for each cephalometric point and for each patient. Accuracy was assessed by how distant (in mm) each time point coordinate was from the respective cephalometric centroid per patient. The average of these differences for all patients was graphed for each cephalometric landmark.

To assess reproducibility, a Bonferroni correlation was calculated for each patient in each of the three dimensions (x,y,z) for all three timepoints. To further increase the evidence of reliability, a Bland-Altman reproducibility test was performed to aid in visualization of point selection between the patients and the three timepoints.

RESULTS

Reliability

The pilot study showed that the minimal difference (less than 4 mm except for point Go1_Lt) existed between each tracing timepoint for each patient. When averaging the difference for each landmark between timepoints for all patients, less than 2.5 mm difference was found to exist among all three tracings timepoints.

The most consistent points between all patients at all time points were the cephalometric landmarks used to define the axis orientations (sella, basion, and nasion) with less than 1-mm difference between all patients at all three timepoints (Figures 35-38). The largest difference of any point from their respective centroid was 0.75-mm (Or_Lt along the x-axis). The majority of cephalometric points were less than 0.5-mm from their respective centroid. This indicates a high level of intra-observer accuracy overall when reproducing the cephalometric points (Table 6).

When assessing the statistical outcome of the Pearson Correlation with Bonferroni correction applied, there was no statistical difference among the five patient's three timepoints with a high level correlation (P<.01; Figure 35).

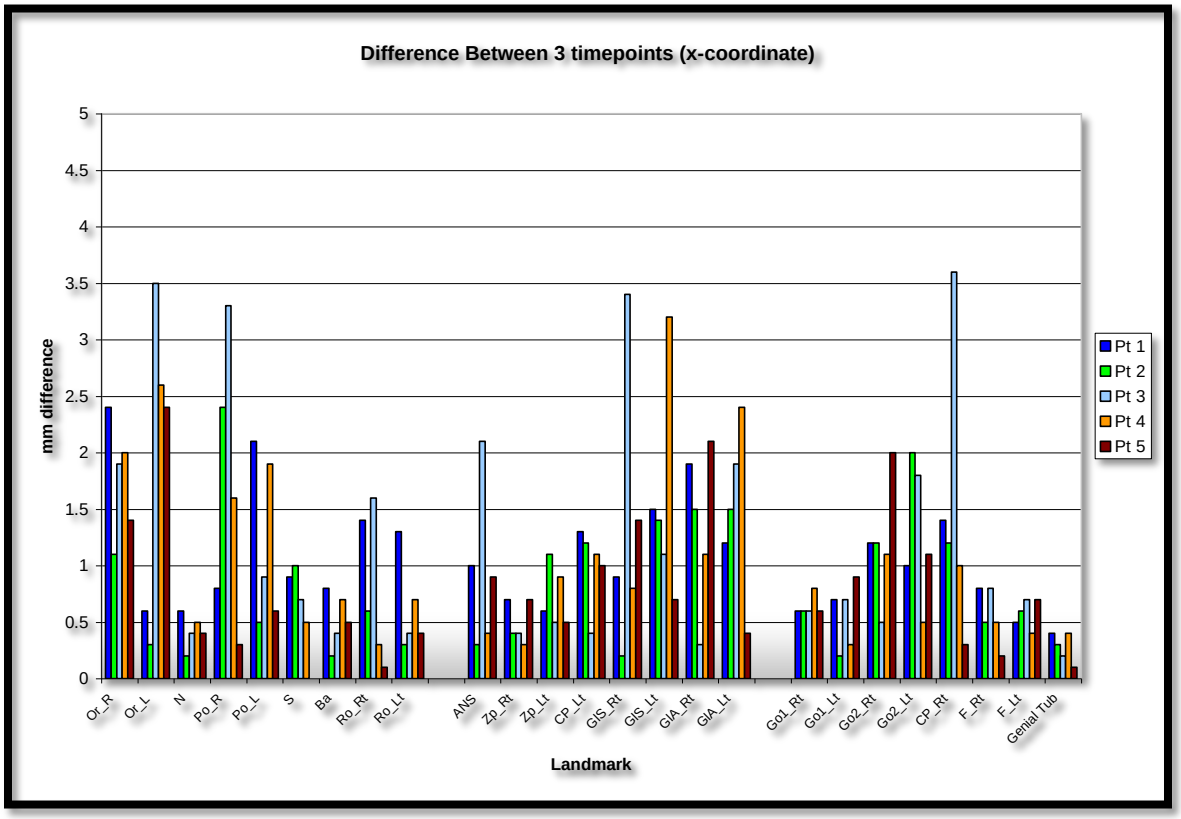

Figure 35: Graph of the differences in a particular measurement along one axis, the x coordinate, for each patient as completed over three timepoints.

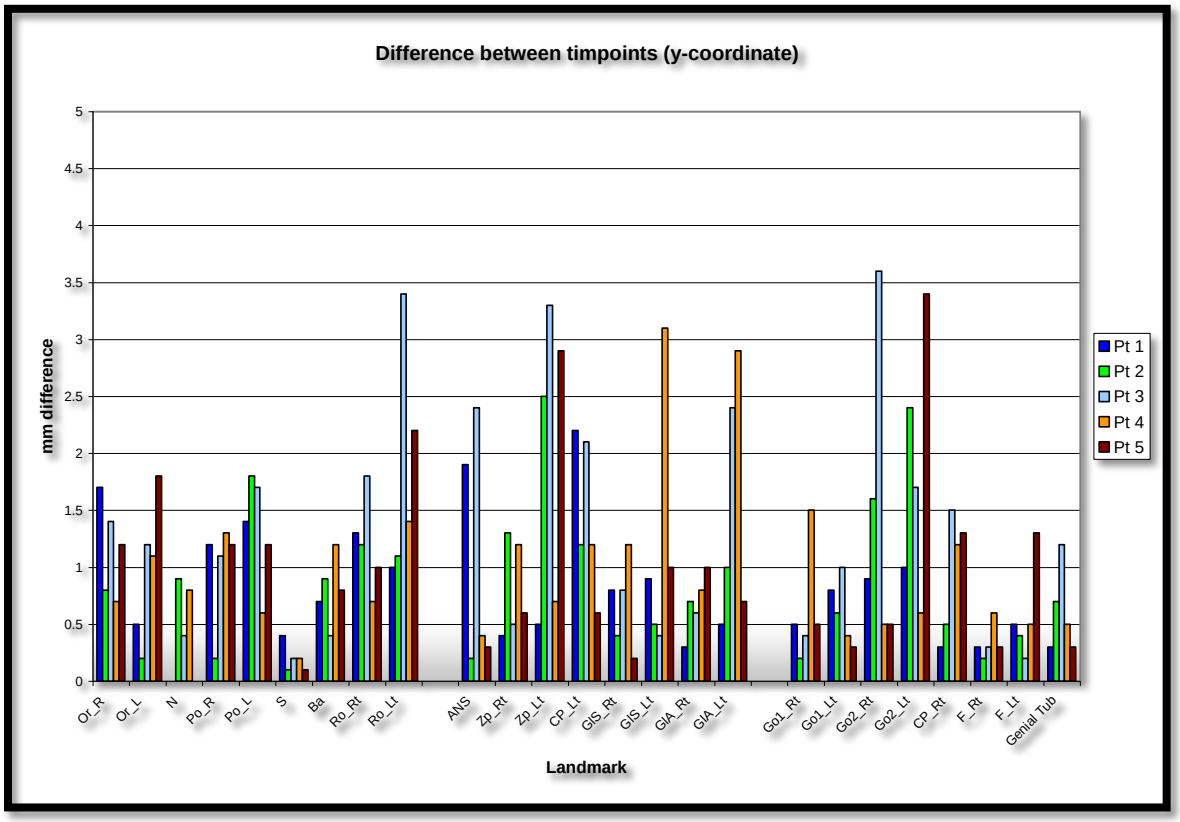

Figure 36: Graph of the differences in a particular measurement along one axis, the y coordinate, for each patient as completed over three timepoints.

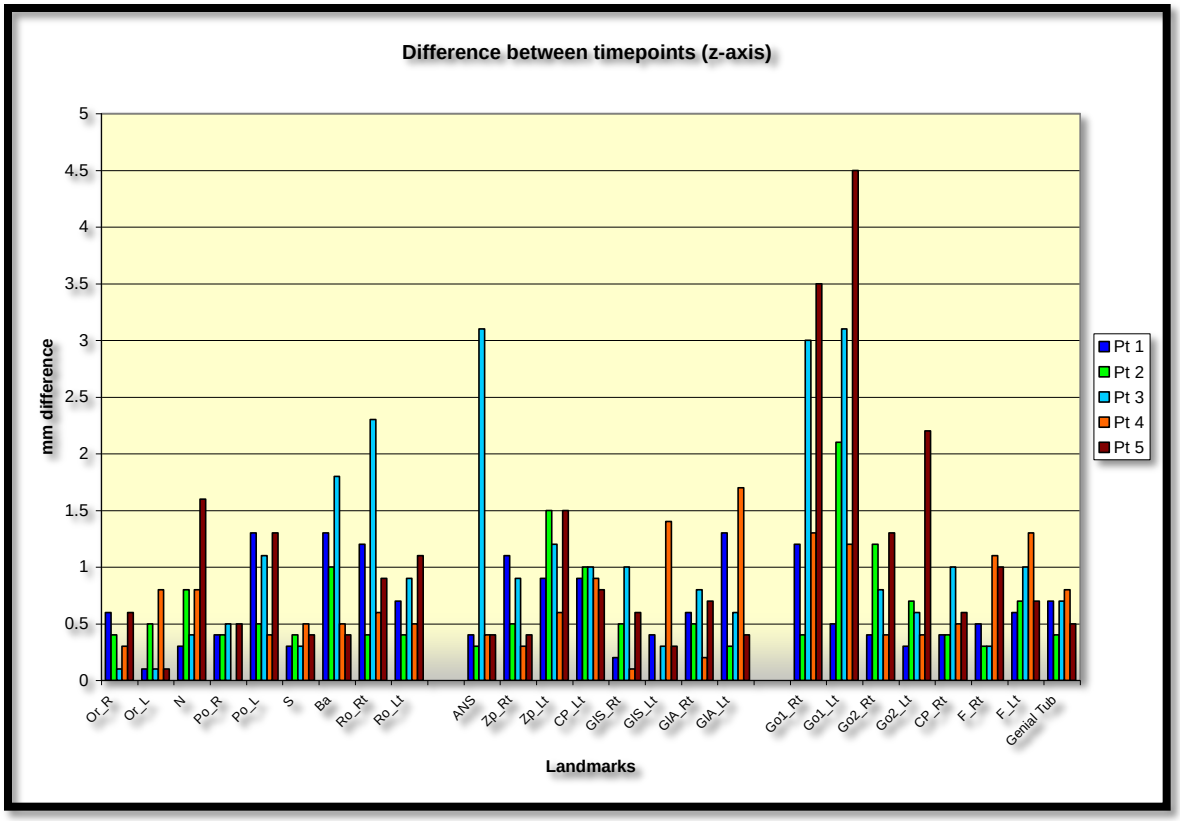

Figure 37: Graph of the differences in a particular measurement along one axis, the z coordinate, for each patient as completed over three timepoints.

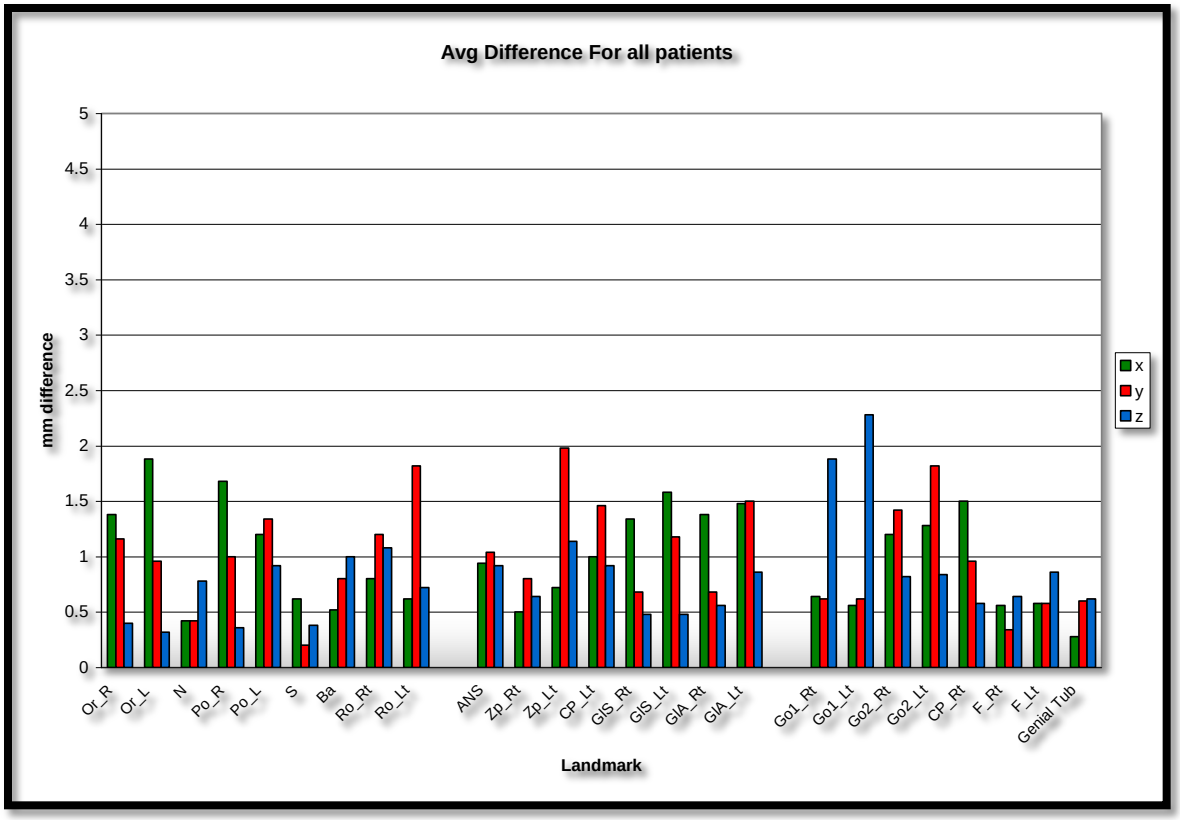

Figure 38: Comparison of the average difference for each landmark in three axes when the measurement was completed over three times.

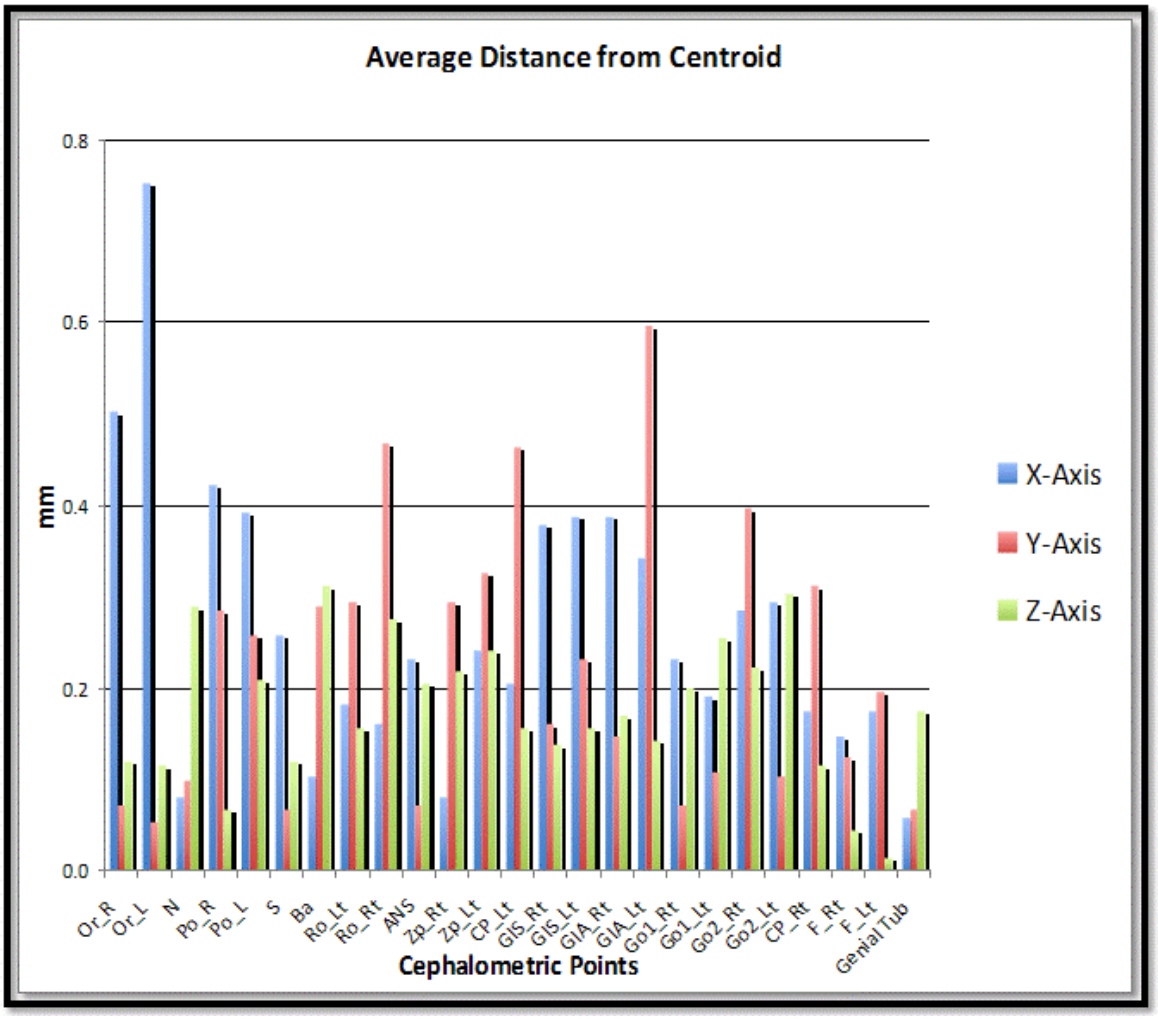

Figure 39: Average distance of each landmark from the centroid for that landmark, measured three times in five patients.

Table 6 Pearson Correlation Coefficient with the applied Bonferroni correction: The correlation of each of the measurements of each of the landmarks measured at three different time points in each patient and then determining the correlation of all points along that coordinate plane.

Patient MR									
	Coordinate								
Timpoint	X1	X2	X3	Y1	Y2	Y3	Z1	Z2	Z3
1	1			1			1		
2	0.9997*	1		0.9997*	1		0.9999*	1	
3	0.9998*	0.9997*	1	0.9997*	0.9998*	1	0.9999*	0.9999*	1
	* denotes P<.01								

Patient RP									
	Coordinate								
Timpoint	X1	X2	X3	Y1	Y2	Y3	Z1	Z2	Z3
1	1			1			1		
2	0.9998*	1		0.9994*	1		0.9997*	1	
3	0.9998*	0.9998*	1	0.9997*	0.9997*	1	0.9999*	0.9998*	1
	* denotes P<.01								

Patient AC									
	Coordinate								
Timpoint	X1	X2	X3	Y1	Y2	Y3	Z1	Z2	Z3
1	1			1			1		
2	0.9993*	1		0.9992*	1		0.9992*	1	
3	0.9998*	0.9995*	1	0.9991*	0.9993*	1	0.9998*	0.9994*	1
	* denotes P<.01								

Patient OS									
	Coordinate								
Timpoint	X1	X2	X3	Y1	Y2	Y3	Z1	Z2	Z3
1	1			1			1		
2	0.9996*	1		0.9993*	1		0.9998*	1	
3	0.9999*	0.9998*	1	0.9997*	0.9995*	1	0.9998*	0.9999*	1
	* denotes P<.01								

Patient AS									
	Coordinate								
Timpoint	X1	X2	X3	Y1	Y2	Y3	Z1	Z2	Z3
1	1			1			1		
2	0.9997*	1		0.9993*	1		0.9988*	1	
3	0.9998*	0.9999*	1	0.9995*	0.9997*	1	0.9998*	0.9989*	1
	* denotes P<.01								

Pooled Patients									
	Coordinate								
Timpoint	X1	X2	X3	Y1	Y2	Y3	Z1	Z2	Z3
1	1			1			1		
2	0.9996*	1		0.9994*	1		0.9995*	1	
3	0.9998*	0.9997*	1	0.9995*	0.9996*	1	0.9998*	0.9997*	1
	* denotes P<.01								

When applying the Bland-Altman test for reproducibility in the three planes over the three timepoints of measurement, the data showed that the measurements for each measure varied less 0.4-mm (Figures 40). For 95% of all pairs of measurements, the absolute difference between the 2 measurements may be as much as $(1.96)(\sigma_{diff}) = (1.96)(1.41)\, s_W = 2.77\, s_W$

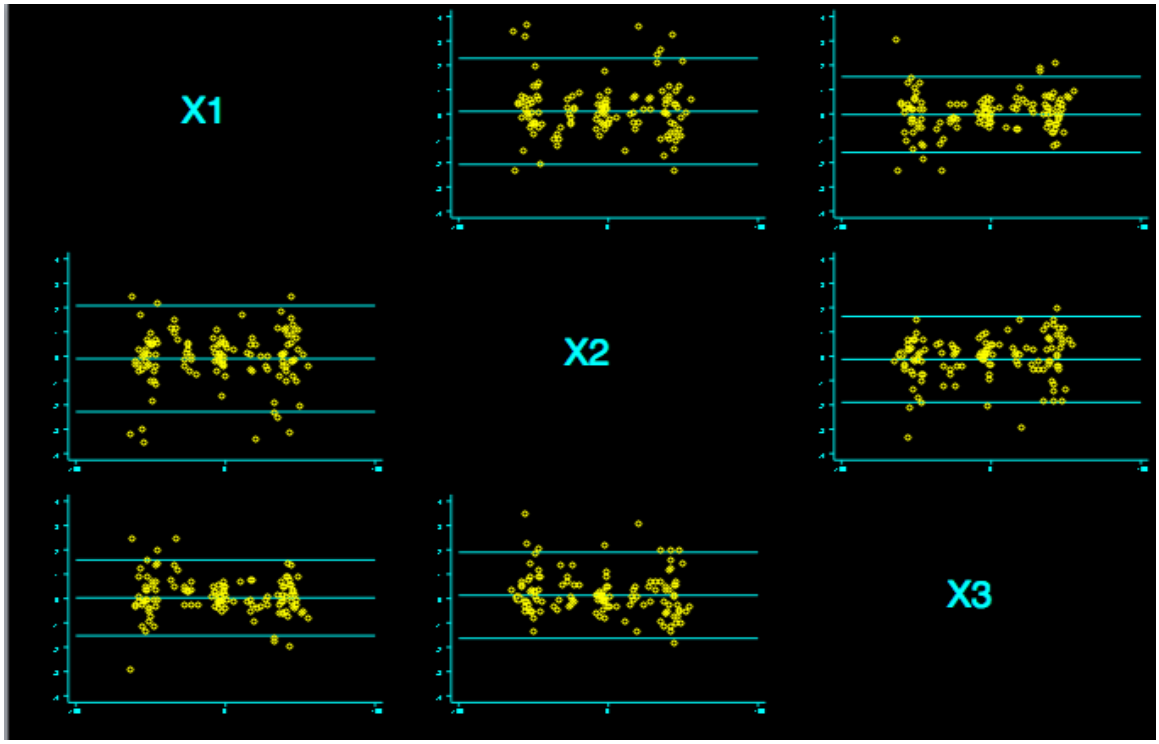

Method 1	Method 2	Mean	[95% Reference Range]		Minimum	Maximum
x2	x1	-0.103	-2.283	2.077	-3.600	2.400
x3	x1	0.028	-1.528	1.584	-3.000	2.400
x3	x2	0.131	-1.636	1.898	-1.900	3.400

Range of x values is -64.05 to 56.15, range of y values is -3.6 to 3.6

Figure 40: Bland-Altman plots comparing all the measurements in the x plane over three different time points in which measurements are compared between two timepoints in each graph with a vertical scale indicating a maximum of 0.4-mm.

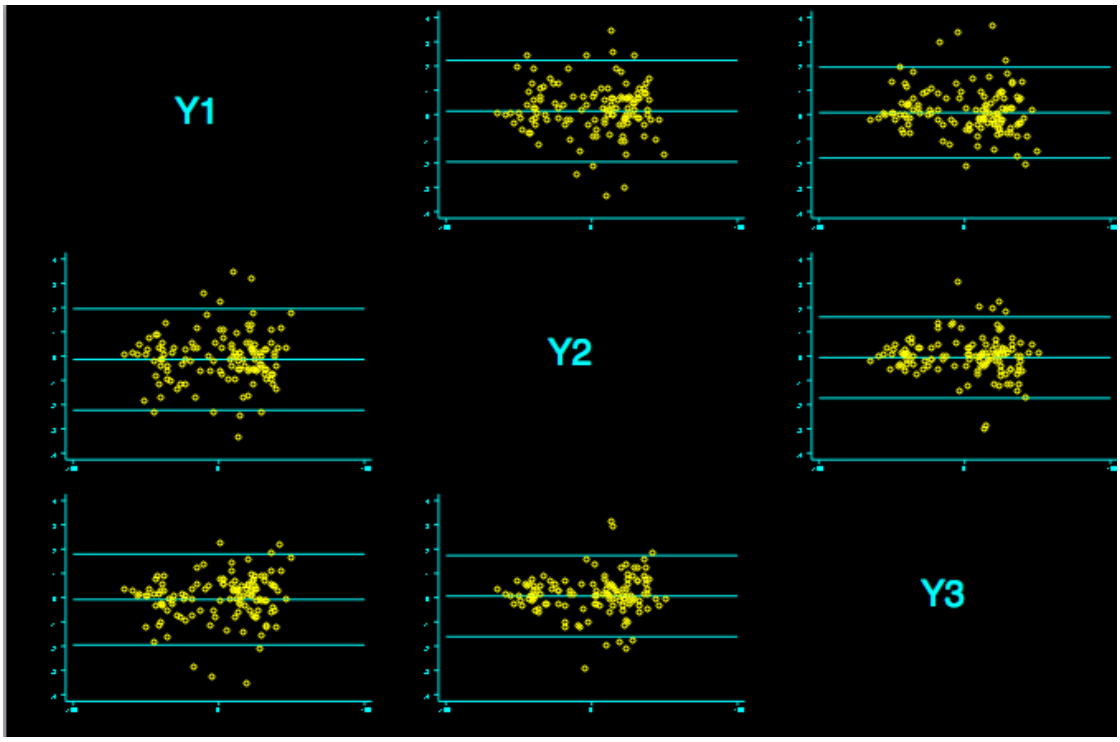

Method 1	Method 2	Mean	[95% Reference Range]		Minimum	Maximum
y2	y1	-0.141	-2.232	1.950	-3.400	3.400
y3	y1	-0.078	-1.951	1.794	-3.600	2.200
y3	y2	0.062	-1.610	1.735	-3.000	3.100

Range of x values is -63.6 to 51.95, range of y values is -3.6 to 3.6

Figure 41: Bland-Altman plots comparing all the measurements in the y plane over three different time points in which measurements are compared between two timepoints in each graph with a vertical scale indicating a maximum of 0.4-mm.

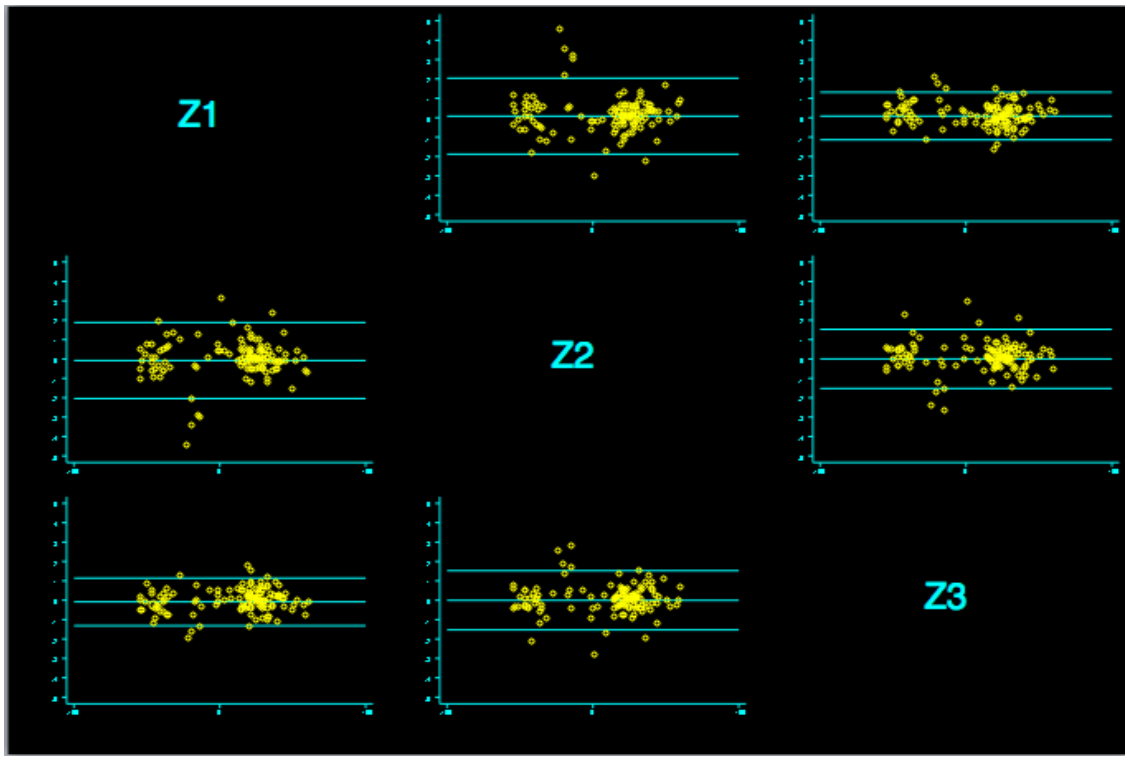

Method 1	Method 2	Mean	[95% Reference Range]		Minimum	Maximum
z2	z1	-0.081	-2.041	1.880	-4.500	3.100
z3	z1	-0.085	-1.311	1.142	-2.000	1.700
z3	z2	-0.004	-1.531	1.523	-2.900	2.700

Range of x values is -53.8 to 61.6, range of y values is -4.5 to 4.5

Figure 42: Bland-Altman plots comparing all the measurements in the z plane over three different time points in which measurements are compared between two timepoints in each graph with a vertical scale indicating a maximum of 0.4-mm.

Final Visual Analysis

The asymmetry analysis was designed so that an investigator and/or clinician could review the frontal view of the patient craniofacial skeleton and, simultaneously, see the quantitative measurements that indicate the actual differences. The program also allowed evaluating

from the rostral to caudal levels in the horizontal plane, and from the anterior to posterior in the sagittal plane, and between the left and right sides from the midline (Figures 43-44). As this example in one patient shows, the investigator has the capability to determine where the asymmetry occurs in any of the three planes. In this patient, the greatest asymmetry occurs in the frontal plane and within the mandible.

Figure 43: Example of the final output from the new analysis which shows the frontal volumetric view of the subject (left) and the quantitative measurements exhibited rostrocaudally with a graph (wigglegram) indicating the major differences.

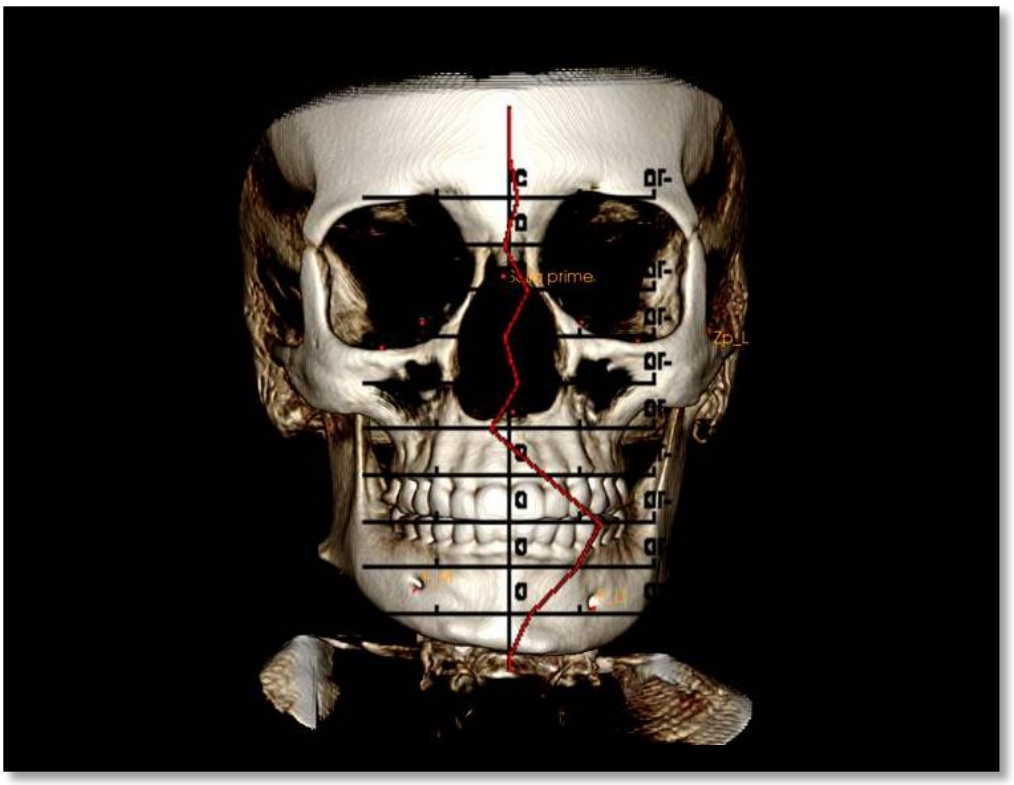

Figure 44: Example of a visual frontal view of the three-dimensional volumetric image of one patient with an overlay of the wigglegram that shows which measurements have the greatest differences between the left and right sides.

DISCUSSION

Choosing points in three-dimensional analysis presents a new set of challenges when compared to landmark selection on two-dimensional x-rays. Depth, width, and height must be taken into account, and depending on the software used to analyze the reconstructed data, density and saturation must also be considered when rendering the hard tissue for viewing. Depending on the depth of the soft tissue and the settings used to take the CBCT, variation can occur in the appearance in the underlying structures.[18]

Various CBCT systems with multiple settings can also cloud the identification of certain landmarks. The voxel size on the given scan can result in differential identification of

structures. As Berco *et al.,* found with their study in linear and angular measurements, scans on the same machines yielded slightly different results, although insignificant statistically.[10] They found the threshold of their measurement error to be under the voxel size, thus attributing to the amount of variation that was seen in their resultant linear measurements to the resolution of the image.

Most points in two-dimensions can be delineated as single points at the intersection of two lines allowing for relatively repeatable identification. When a third dimension is introduced into the equation, points must now be chosen on curved, sloping structures. One must also take into consideration the cost/benefit ratio as well the increased dosage that is associated with taking CBCT images.[3, 19]

Having the majority of measurements made from a landmark to one of the three origin planes allowed the investigator to separate right/left, superior/inferior, and anterior/posterior in terms of orientation of each landmark. This created identification of bilateral structures and their orientation to their ipsilateral counterpart. The final illustration of the "wiggle-gram" provides both the numerical deviation from each ipsilateral landmark as well as diagrammatic evidence to which side the difference occurs with a relative magnitude as visualized by the deviation of the red line from the specific plane (mid-sagittal, horizontal, etc.).

Limitations of the Study

A small group of study patients could have affected the reproducibility of the landmarks as well as only one observer traced all patients. All patients were scanned on the same CBCT machine, and as such, contrast and density were altered for optimal hard tissue viewing based on the software's interpretation of the rendered data. Manual manipulation of the patient must be done by the investigator to redefine certain visual parameters in order to properly identify all landmarks, allowing for some variability each time in the amount of contrast/saturation/density that is used as well as the orientation of the individual within the software.

Although there seemed to be some variability when selecting the points to determine the origin and axis, any variation in each essential point selected (*i.e.,* points on which the axis are based) has little effect on the orientation of the axis. For example, Orbitale Right has a wider variation overall in patients, but only along the x axis, which has zero effect on the final orientation of the axis. A similar finding in Orbitale was found in the study by Lagravère *et al.,* It was seen that the identification of both Orbitale and Porion could vary by roughly as much as 2-mm for Orbitale and at least 5-mm for Porion in the x-direction[16, 20]. However, Orbitale's detection in the z-direction (the direction in which it is important for the establishment of the Ulrich Analysis) was also found to have little variation similar to the current study's findings.

As the pilot study shows, Patient 3 had a larger amount of variation when attempting to repeat landmark identification among all points compared to the other four patients. This error may be due to the fact this patient had a significant craniofacial asymmetry making certain structures more variable in their appearance and more difficult to determine the site of the landmark.

When looking at the centroid's placement, both Orbitale landmarks as well as the glenoid fossa inferior/articular eminence showed a higher rate of variability than the other points. Schlicher *et al.,* [17] found similar difficulties when analyzing the results with orbitale in his study with 9 different raters, finding a 1.81-mm average difference between raters. It was found during manipulation within the software, that orbitale's physical location along the x-axis was highly susceptible to movement when altering the brightness or contrast. Fortunately, this movement had no influence on the orientation of the axis, as movement along the horizontal plane only effects lateral vectors, with no other effect on other aspects of orientation.

Although physical limitations as to the difficulty of landmark identification of the study are present, it must not overshadow the statistical significance of the reproducibility of the landmarks. As no statistically significant difference was found for any of the patients between timepoints in terms of landmark identification, a few criticisms of the statistics used must be discussed. The Pearson correlation coefficient is overly conservative in terms of a measurement of agreement, if not used with a correction such as the Bonferroni. While the use of Bonferroni correction decreases the conservative nature of the Pearson correlation, it

opens the doors for false negatives, reducing the power of the statistic. It lacks specificity at calculating intra-rater reliability for individual landmarks, but did provide a method to account for the agreement of timepoints. The construction of a centroid allowed for an associative comparison of each individual landmark to each timepoint as well as a relative correlation to the accuracy of the rater's identification of all points along their individual axis (*i.e.*, in x, y, z planes). However, even if the existence of a centroid identifies that an error has occurred between timepoints for each landmark selection, its presence in relation to the differing coordinates is merely a relative estimate to the consistency one has in choosing a point in three-dimensional space. The Bland-Altman test for reproducibility took the approach of the centroid a step further allowing for estimates of the error that could exist when identifying points along any axis comparing all timepoints and landmarks for all five patients. Once again, considering the test's capability to look at all coordinates along a single plane with all patients, the amount of error represents the extreme cases and does not take into account the individual patient, but rather the entire pool of coordinates from all pilot patients.

Future Work

This study was designed to provide a three-dimensional method of analysis of craniofacial asymmetry as well as a transition from two-dimensional x-ray images to three-dimensional cone beam computed tomography images. This orientation scheme combined with a simple asymmetry analysis is constructed for the purpose of future modification by investigators and clinicians, and for promoting further use of three-dimensional analysis in orthodontics. The establishment of 3D imaging and analysis in orthodontics is still developing, and with the

sizable amount of data available from a single image, it is impossible to encompass all aspects of analysis or to incorporate all there is to be gleaned from such information. Ultimately, the proposed analysis in this study will invoke thought and spur controversy as to its validity and usefulness. However, with further work and future studies, much more can be developed from this early study that will continually encourage those to evolve, reshape, and tailor an analysis that suites their preferences. As the British poet Philip Ayers stated, "Make falling arts your care, erect new wonders, and the old repair…call forth th' idea's of your mind, proud to accomplish what such hands design'd."

REFERENCES

1. Cattaneo, P.M. and B. Melsen, *The use of cone-beam computed tomography in an orthodontic department in between research and daily clinic.* World J Orthod, 2008. **9**(3): p. 269-82.
2. Quintero, J.C., et al., *Craniofacial imaging in orthodontics: historical perspective, current status, and future developments.* Angle Orthod, 1999. **69**(6): p. 491-506.
3. Hatcher, D.C., *Operational principles for cone-beam computed tomography.* J Am Dent Assoc. **141 Suppl 3**: p. 3S-6S.
4. Kapila, S., R.S. Conley, and W.E. Harrell, Jr., *The current status of cone beam computed tomography imaging in orthodontics.* Dentomaxillofac Radiol. **40**(1): p. 24-34.
5. Chan, H.J., M. Woods, and D. Stella, *Three-dimensional computed craniofacial tomography (3D-CT): potential uses and limitations.* Aust Orthod J, 2007. **23**(1): p. 55-64.
6. Kau, C.H., et al., *Three-dimensional cone beam computerized tomography in orthodontics.* J Orthod, 2005. **32**(4): p. 282-93.
7. Smith, B.R., J.H. Park, and R.A. Cederberg, *An evaluation of cone-beam computed tomography use in postgraduate orthodontic programs in the United States and Canada.* J Dent Educ. **75**(1): p. 98-106.
8. Cattaneo, P.M., et al., *Comparison between conventional and cone-beam computed tomography-generated cephalograms.* Am J Orthod Dentofacial Orthop, 2008. **134**(6): p. 798-802.

9. Sanders, D.A., et al., *Skeletal and dental asymmetries in Class II subdivision malocclusions using cone-beam computed tomography.* Am J Orthod Dentofacial Orthop. **138**(5): p. 542 e1-20; discussion 542-3.

10. Berco, M., et al., *Accuracy and reliability of linear cephalometric measurements from cone-beam computed tomography scans of a dry human skull.* Am J Orthod Dentofacial Orthop, 2009. **136**(1): p. 17 e1-9; discussion 17-8.

11. Park, S.H., et al., *A proposal for a new analysis of craniofacial morphology by 3-dimensional computed tomography.* Am J Orthod Dentofacial Orthop, 2006. **129**(5): p. 600 e23-34.

12. El-Beialy, A.R., et al., *Accuracy and reliability of cone-beam computed tomography measurements: Influence of head orientation.* Am J Orthod Dentofacial Orthop. **140**(2): p. 157-65.

13. Kumar, V., et al., *Comparison of conventional and cone beam CT synthesized cephalograms.* Dentomaxillofac Radiol, 2007. **36**(5): p. 263-9.

14. Yanez-Vico, R.M., et al., *Diagnostic of craniofacial asymmetry. Literature review.* Med Oral Patol Oral Cir Bucal. **15**(3): p. e494-8.

15. Arat, Z.M., et al., *Longitudinal growth changes of the cranial base from puberty to adulthood. A comparison of different superimposition methods.* Angle Orthod. **80**(4): p. 537-44.

16. Lagravere, M.O., et al., *Intraexaminer and interexaminer reliabilities of landmark identification on digitized lateral cephalograms and formatted 3-dimensional cone-beam computerized tomography images.* Am J Orthod Dentofacial Orthop. **137**(5): p. 598-604.

17. Schlicher, W., et al., *Consistency and precision of landmark identification in three-dimensional cone beam computed tomography scans.* Eur J Orthod.

18. Lou, L., et al., *Accuracy of measurements and reliability of landmark identification with computed tomography (CT) techniques in the maxillofacial area: a systematic review.* Oral Surg Oral Med Oral Pathol Oral Radiol Endod, 2007. **104**(3): p. 402-11.

19. Curley, A. and D.C. Hatcher, *Cone beam CT--anatomic assessment and legal issues: the new standards of care.* J Calif Dent Assoc, 2009. **37**(9): p. 653-62.

20. Lagravere, M.O., et al., *Reliability of traditional cephalometric landmarks as seen in three-dimensional analysis in maxillary expansion treatments.* Angle Orthod, 2009. **79**(6): p. 1047-56.

Publishing Agreement

It is the policy of the University to encourage the distribution of all theses, dissertations, and manuscripts. Copies of all UCSF theses, dissertations, and manuscripts will be routed to the library via the Graduate Division. The library will make all theses, dissertations, and manuscripts accessible to the public and will preserve these to the best of their abilities, in perpetuity.

Please sign the following statement:

I hereby grant permission to the Graduate Division of the University of California, San Francisco to release copies of my thesis, dissertation, or manuscript to the Campus Library to provide access and preservation, in whole or in part, in perpetuity.

Author Signature

06/05/12

Date